Journal Pre-proof

Conjugable A_3 adenosine receptor antagonists for the development of functionalized ligands and their use in fluorescent probes

Stephanie Federico, Enrico Margiotta, Stefano Moro, Eszter Kozma, Zhan-Guo Gao, Kenneth A. Jacobson, Giampiero Spalluto

PII: S0223-5234(19)31038-4

DOI: https://doi.org/10.1016/j.ejmech.2019.111886

Reference: EJMECH 111886

To appear in: *European Journal of Medicinal Chemistry*

Received Date: 18 September 2019

Revised Date: 12 November 2019

Accepted Date: 12 November 2019

Please cite this article as: S. Federico, E. Margiotta, S. Moro, E. Kozma, Z.-G. Gao, K.A. Jacobson, G. Spalluto, Conjugable A_3 adenosine receptor antagonists for the development of functionalized ligands and their use in fluorescent probes, *European Journal of Medicinal Chemistry* (2019), doi: https://doi.org/10.1016/j.ejmech.2019.111886.

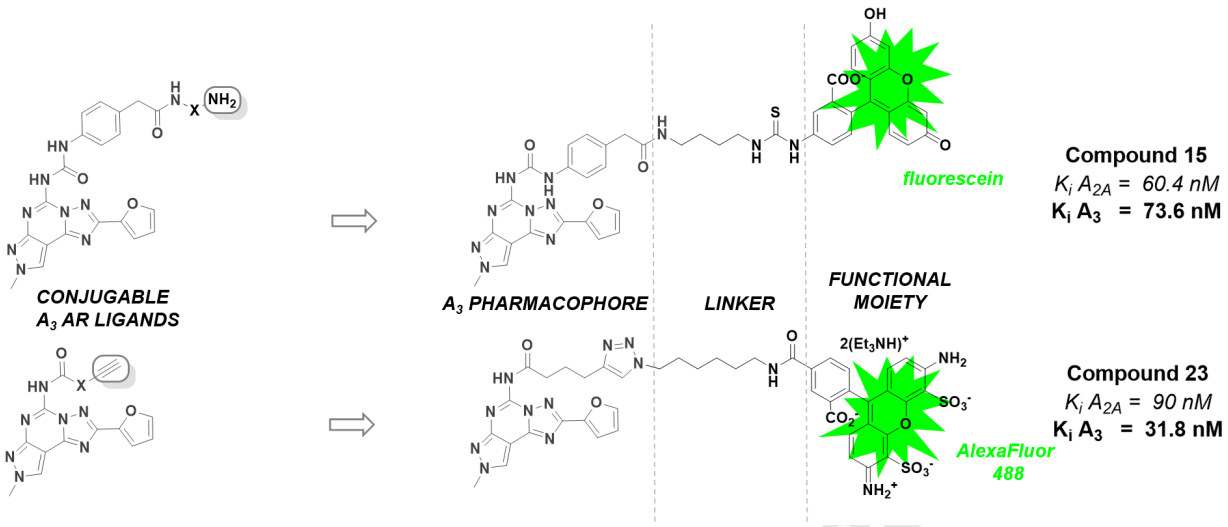

Compound 15
K_i A_{2A} = *60.4 nM*
K_i A_3 = 73.6 nM

Compound 23
K_i A_{2A} = *90 nM*
K_i A_3 = 31.8 nM

Conjugable A_3 adenosine receptor antagonists for the development of functionalized ligands and their use in fluorescent probes

Stephanie Federico, *[#] Enrico Margiotta, [§] Stefano Moro, [§] Eszter Kozma, [≠] Zhan-Guo Gao, [≠] Kenneth A. Jacobson, [≠] and Giampiero Spalluto[#]

[#]*Dipartimento di Scienze Chimiche e Farmaceutiche, Università degli Studi di Trieste, Via Licio Giorgeri 1, 34127 Trieste, Italy*

[§]*Molecular Modeling Section (MMS), Dipartimento di Scienze del Farmaco, Università di Padova, via Marzolo 5, 35131 Padova, Italy*

[≠]*Laboratory of Bioorganic Chemistry, NIDDK, National Institute of Health, Bethesda, Maryland, USA*

To whom correspondence should be addressed.

Tel +39 040 5583671 (S.F.), Fax +39 040 5583903, E-mail: sfederico@units.it

Keywords: G protein-coupled receptor; adenosine receptors; fluorescent ligands; molecular modeling; molecular probes.

Abbreviations: AR, adenosine receptor; BOC, *tert*-butyloxycarbonyl; EDCI, 1-ethyl-3-(3-dimethylaminopropyl)carbodiimide; FITC, fluorescein isothiocyanate; PTP, pyrazolo[4,3-*e*]-1,2,4-triazolo[1,5-*c*]pyrimidine;

Abstract

Compounds able to simultaneously bind a biological target and be conjugated to a second specific moiety are attractive tools for the development of multi-purpose ligands useful as multi-target ligands, receptor probes or drug delivery systems, with both therapeutic and diagnostic applications. The human A_3 adenosine receptor is a G protein-coupled receptor involved in many physio-pathological conditions, e.g. cancer and inflammation, thus representing a promising research target. In this work, two series of conjugable hA_3AR antagonists, based on the pyrazolo[4,3-*e*]-1,2,4-triazolo[1,5-*c*]pyrimidine nucleus, were developed. The introduction of an aromatic ring at the 5 position of the scaffold, before (phenylacetamido moiety) or after (1,2,3-triazole obtained by click chemistry) the conjugation is aimed to increase affinity and selectivity towards the hA_3AR receptor. As expected, conjugable compounds showed good affinity towards the hA_3AR. In order to prove their potential in the development of hA_3AR ligands for different purposes, compounds were also functionalized with fluorescent probes. Unfortunately, conjugation decreased affinity and selectivity for the target as compared to the $hA_{2A}AR$. Computational studies identified specific non-conserved residues of the extracellular loops which constitute a structural barrier able to discriminate between ligands, giving insights into the rational development of new highly selective ligands.

Introduction

Activation or blockade of adenosine receptors (ARs) are responsible for diverse pharmacological effects in various tissues and organs. Considering the wide distribution of endogenous adenosine, it is generally accepted that the regulation of ARs has great therapeutic potential [1–6].

ARs are members of the superfamily of G protein-coupled receptors (GPCRs), and four subtypes are currently known, named A_1AR, A_{2A}AR, A_{2B}AR, and A_3AR [7]. In recent decades, numerous medicinal chemistry groups have developed promising ligands, agonists and antagonists for these receptor subtypes [8]. In particular, the search for selective antagonists held greater appeal than selective agonists, not only for their potential therapeutic applications but also for their preferential use as molecular probes for pharmacological characterization of receptors [9].

In this field, our research group and others have extensively investigated the pyrazolo[4,3-*e*]-1,2,4-triazolo[1,5-*c*]pyrimidine nucleus (PTP) that, by appropriate modifications at the N7, N8, and 5 positions, led to very potent and selective human (h) A_{2A} and A_3 AR antagonists [10–16]. These derivatives have previously been used for the study of the functional role of A_{2A} and A_3 ARs, in particular through the preparation of radiolabeled or irreversible derivatives [17–21]. Nevertheless, another interesting approach for the investigation of AR subtypes could be considered the functionalization of the PTP scaffold with spacers able to link various groups such as fluorophore or nanoparticles for drug delivery [22–32].

Using the PTP scaffold we have recently reported a new series of derivatives of general formulae **1**, in which a diamino moiety of different lengths was introduced at the 5 position. Using this approach, a new series of derivatives bearing a fluorophore group linked to the free amino group was reported as potential fluorescent probes (Figure 1) [33].

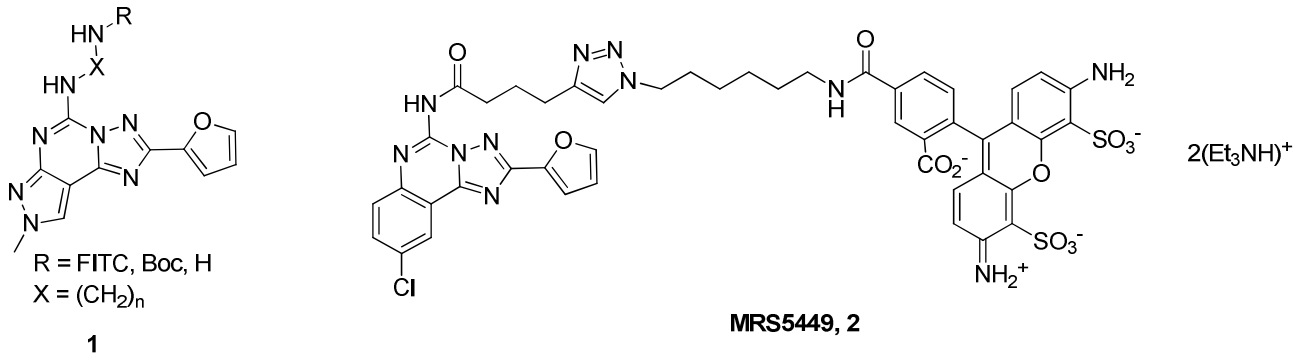

Figure 1. Structures of previously reported AR antagonists and reference compounds.

In this work, we explored the structure activity relationship (SAR) of conjugable AR ligands useful for

the development of probes selective for the hA_3AR. In addition to their usefulness to better define the specific role of the target protein in both physiological and pathological processes, availability of hA_3AR selective probes could be used for diagnostic purposes. In fact, hA_3AR was found to be overexpressed in certain cancers, such as melanoma and breast and colorectal cancer, and the overexpression level well correlates with the severity of the tumor, thus making it a possible biomarker of such tumors [34–38]. Unfortunately, the previously synthesized PTP derivatives generally showed a poor affinity for the hA_3AR and low A_3AR selectivity versus the other receptor subtypes [33]. A possible explanation of lack of affinity and selectivity of these compounds could be attributed to the absence of an aromatic moiety at the 5 position, which previous studies indicated to be important for both affinity and selectivity at the hA_3AR [10].

Taking into account these experimental observations and with the aim of improving selectivity versus the hA_3AR subtype, we decided to design a new series of conjugable PTPs bearing an aromatic portion at the 5 position (**3-18**) and anchored to chains of different lengths. These chains act as spacers and at their terminal position bear a functional group for subsequent functionalization. On the basis of our modeling of the AR interactions of PTP ligands, the most reliable orientation of the linker is towards the extracellular loops (ELs) of the receptors [33]. This means that any difference in sequence and conformation of the ELs of the AR subtypes could affect either selectivity or affinity through direct ligand interaction. Indeed, our recent work about the selection of the best template for hA_3AR homology modeling highlighted that EL region displays the highest sequence variability between the hA_1, $hA_{2A,}$ and hA_3AR subtypes [39], suggesting that the ligand partitioning between the ELs and the hydrophobic cavity is crucial for binding.

Thus, finally, we decided to conjugate the new functionalized AR ligands with a fluorescent moiety (e.g. fluorescein) that is able to protrude in the extracellular side, giving new leads for the development of hA_3AR fluorescent probes (Figure 2).

Alternatively, a parallel series of N5 alkynyl functionalized antagonists (**19-22**) was prepared as precursors for copper(I)-catalyzed azide-alkyne (click) cycloaddition. Based on previous studies performed on the triazoloquinazoline nucleus of the nonseletive antagonist CGS15943, which led to a potent and selective fluorescent hA_3AR antagonists (MRS5449, **2**, Figure 1) [40], a fluorophore (e.g. Alexa Fluor-488) was introduced to afford potential A_3AR fluorescent antagonist **23** (Figure 2).

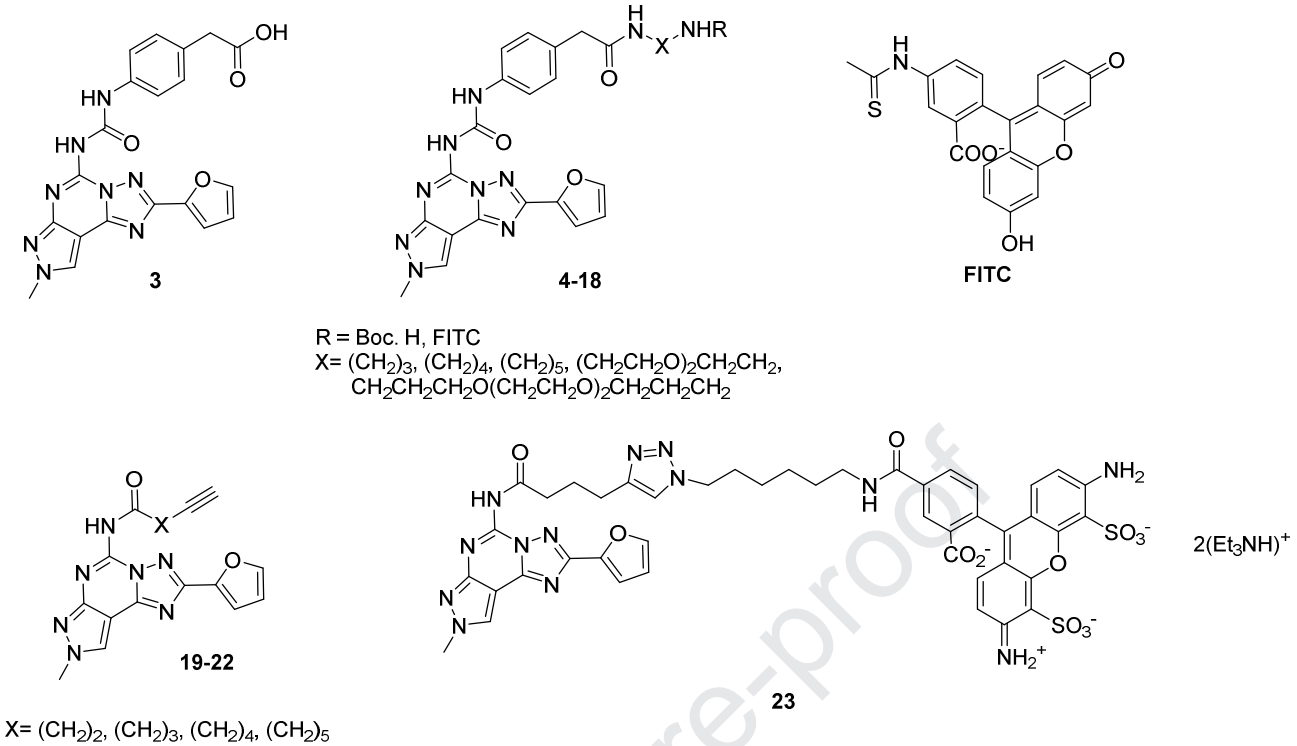

Figure 2. Structures of the synthesized PTP derivatives.

Chemistry

All the designed compounds **3-23** have been synthesized as summarized in Schemes 1-3 [41]. Saponification with lithium hydroxide of previously reported PTP ester derivative **24** [42] led to the corresponding carboxylic acid **3**, which after condensation in presence of EDCI with the appropriate mono BOC-protected diamine **25-29** afforded the desired functionalized compounds **4-8**. A common BOC deprotection with trifluoroacetic acid in dichloromethane provided the free amino compounds **9-13** as salts. Then, after coupling with fluorescein isothiocyanate (FITC) in methanol under an argon atmosphere, the final compounds **14-18** were obtained. (Scheme 1)

Alkynyl PTP derivatives **19-22** were instead prepared by reacting the free amino PTP derivative **30** with the appropriate acyl chlorides **35-38** which were obtained by treatment of the corresponding carboxylic acids **31-34** with oxalyl chloride (Scheme 2).

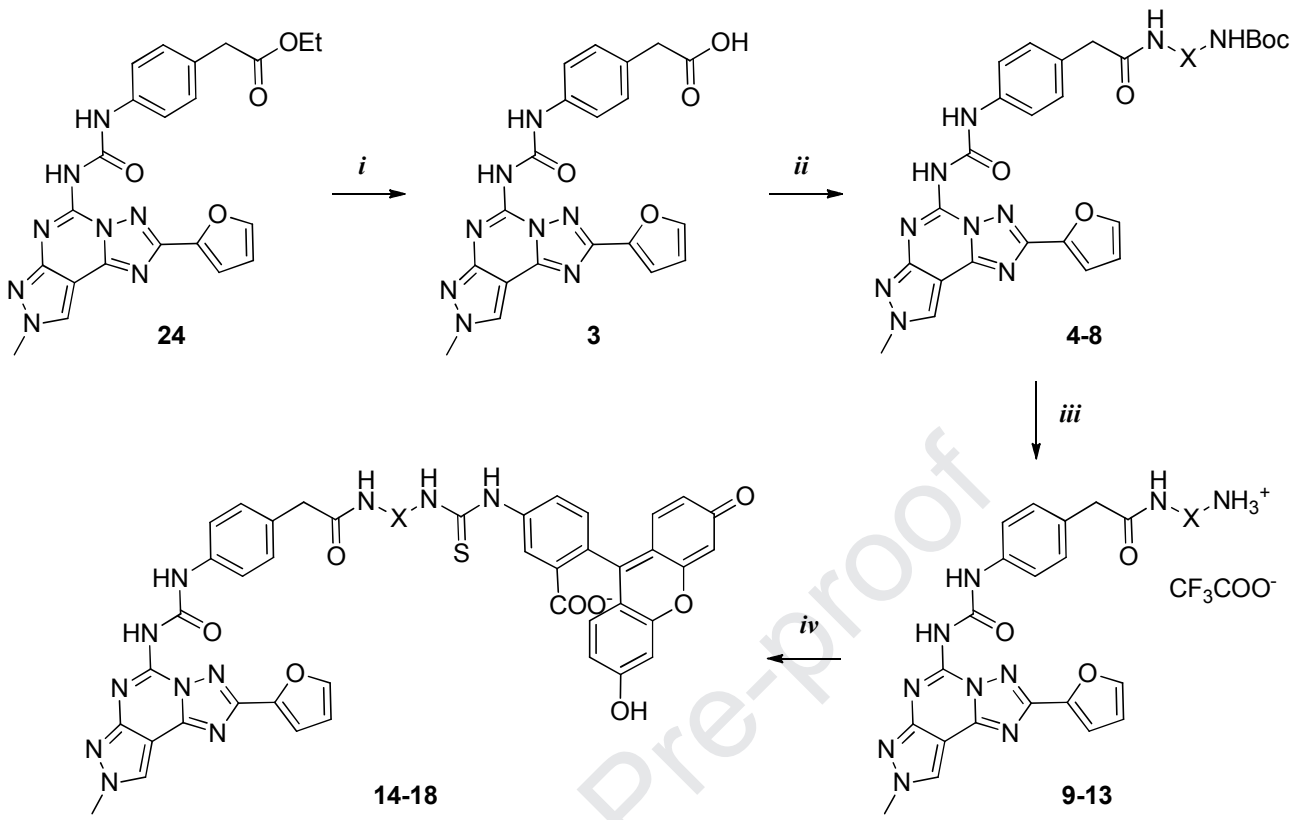

X= $(CH_2)_3$, $(CH_2)_4$, $(CH_2)_5$, $(CH_2CH_2O)CH_2CH_2$, $(CH_2)_3O(CH_2CH_2O)_2(CH_2)_3$

Scheme 1. Synthesis of fluorescent adenosine receptor ligands **14-18.** *Reagents and conditions*: *i*: LiOH, THF, MeOH, water, rt. overnight; *ii*: $NH_2XNHBoc$ (25-29), EDCI, DMAP, DMF, rt, overnight; *iii*: TFA, DCM, rt, 2h; *iv*: FITC, TEA, MeOH, rt, 72h.

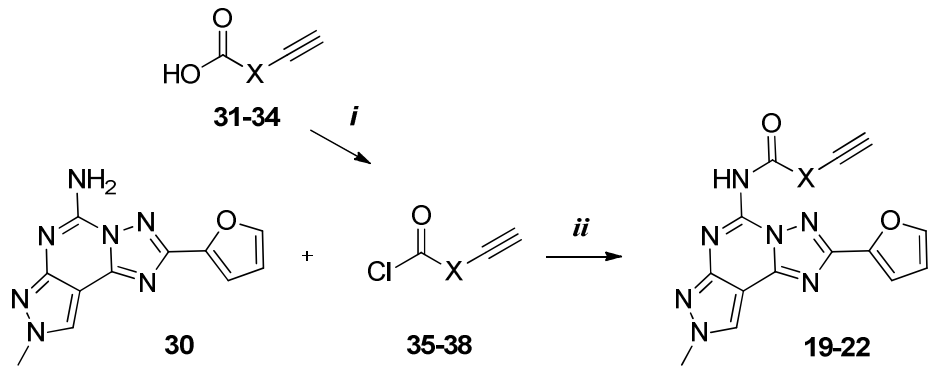

X= $(CH_2)_2$, $(CH_2)_3$, $(CH_2)_4$, $(CH_2)_5$

Scheme 2. Synthesis of alkyne derivatives **19-22**. *Reagents and conditions: i*: oxalyl chloride, DMF cat., $CDCl_3$, 0°C to rt, 3 h; *ii*: TEA. dioxane, reflux, overnight.

The final derivative **23** was prepared by reacting the alkynyl derivative **22** with Alexa Fluor-488 5-carboxamido (6-azidohexanyl)bis(triethylammonium salt) in DMF [40]. (Scheme 3)

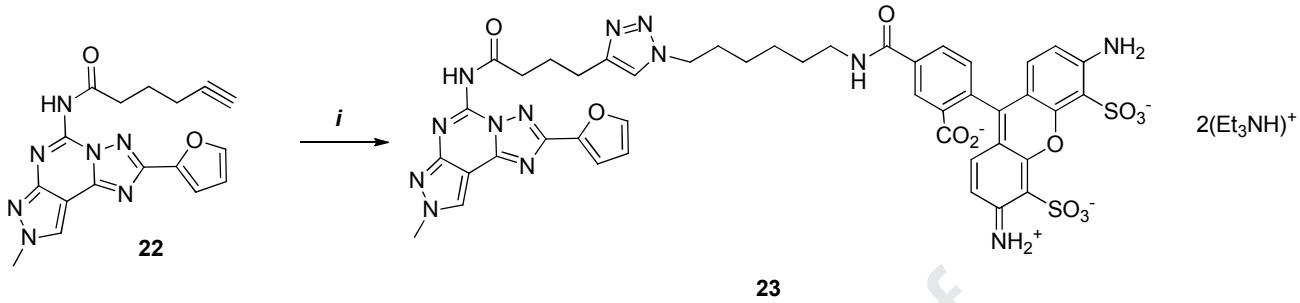

22 **23**

Scheme 3. Synthesis of Alexa Fluor-488 fluorescent AR ligand **23**. *Reagents and conditions: i*: Alexa Fluor 488 5-carboxamido-(6-azidohexanyl) bis(triethylammonium salt), aq. sodium ascorbate, aq. cupric sulfate pentahydrate solution, water, DMF, rt, overnight.

Results and Discussion

Newly synthesized compounds (**3-23**) were tested at the hA_1, hA_{2A} and hA_3 ARs expressed in CHO (hA_1AR, hA_3AR) and HEK293 ($hA_{2A}AR$) cells: [^{3}H]RPIA (hA_1AR), [^{3}H]CGS21680 ($hA_{2A}AR$) and [^{125}I]AB-MECA (hA_3AR) were used as radioligands in binding assays (Table 1) [40,43].

Table 1. Binding profile of synthesized compounds **3-23** at the hA_1, hA_{2A} and hA_3 ARs (see figure 2 for compounds' structures).

Compd	X	R	hA_1 [a]	hA_{2A} [b]	hA_3 [c]	hA_1/hA_3	hA_{2A}/hA_3	hA_1/hA_{2A}
3	-	-	*4%*	1,010	128	> 78	7.8	> 10
4	$(CH_2)_3$	Boc	*15%*	150	2.75	> 3,636	54.5	> 66
5	$(CH_2)_4$	Boc	*2%*	304	3.46	> 2,890	88	> 33
6	$(CH_2)_5$	Boc	*14%*	376	4.47	> 2,237	84.1	> 26.5
7	$(CH_2CH_2O)_2CH_2CH_2$	Boc	*7%*	456	74.8	> 133.6	6.1	> 22
8	$(CH_2)_3O(CH_2CH_2O)_2(CH_2)_3$	Boc	*11%*	327	82.4	> 121.3	3.9	> 30.5
9	$(CH_2)_3$	H[d]	*9%*	175	8.06	> 1,240	21.7	> 57

10	$(CH_2)_4$	H[d]	*4%*	172	6.00	> 1,666	28.6	> 58
11	$(CH_2)_5$	H[d]	*6%*	203	2.66	> 3,759	76.3	> 49
12	$(CH_2CH_2O)_2CH_2CH_2$	H[d]	*17%*	267	19.2	> 520	14	> 37.4
13	$(CH_2)_3O(CH_2CH_2O)_2(CH_2)_3$	H[d]	*1%*	328	10.3	> 970	30.3	> 30
14	$(CH_2)_3$	FITC	*27%*	110	104	> 96	1	> 96
15	$(CH_2)_4$	FITC	*28%*	60.4	73.6	> 23.7	0.82	> 129
16	$(CH_2)_5$	FITC	*21%*	106	96.7	> 103	1.1	> 94
17	$(CH_2CH_2O)_2CH_2CH_2$	FITC	*29%*	95.7	137	> 73	0.69	> 94
18	$(CH_2)_3O(CH_2CH_2O)_2(CH_2)_3$	FITC	*32%*	91.5	207	> 48	0.44	> 109
19	$(CH_2)_2$	-	*55%*	133	11.0	> 909	16.5	> 2.34
20	$(CH_2)_3$	-	n.d.	199	4.11	-	48.4	-
21	$(CH_2)_4$	-	891	151	7.26	122.7	20.7	5.9
22	$(CH_2)_5$	-	*62%*	482	12.8	> 781	37.6	> 20.7
23[e]	-	-	n.d.	90	31.8	-	2.83	-

[a]Displacement of specific [^{3}H]R-PIA binding at hA_1AR expressed in CHO cells, (n=3-6). [b]Displacement of specific [^{3}H]CGS21680 binding at $hA_{2A}AR$ expressed in CHO cells, (n=3-6). [c]Displacement of specific [^{125}I]-AB-MECA binding at hA_3AR expressed in CHO cells, (n=3-6). Data are expressed as Ki (nM) or as % of inhibition (in italics) at a 10 μM concentration of radioligand. n.d. Not determined. Data complete of SEM are reported in ESI (Table S1). [d] Compounds as TFA salts. [e] MRS5763.

As clearly summarized in Table 1, all the synthesized ureido (**3-18**) and amido (**19-23**) compounds showed affinities at the hA_3AR ranging from high nanomolar to nanomolar concentrations, with different degrees of selectivity versus the other subtypes.

The presence of a carboxylic group at the 5 position of compound **3** led to affinity values of 128 nM at the hA_3AR and 1.01 μM at the $hA_{2A}AR$, while it was inactive at the hA_1AR (4% of radioligand displacement at 10 μM). Among all the series, compound **3** is the only one to exhibit a micromolar affinity against the $hA_{2A}AR$, suggesting that the carboxylic moiety is involved in interactions with

different key residues in the orthosteric binding site of the AR subtypes, which are, thus, responsible for the observed selectivity.

Conjugation of the acid moiety with the mono-*N*-BOC protected diamino spacers led to compounds **4-8** which showed high affinity for the hA_3AR (Table 1). It should be noted that the length of the diamino spacer could be a major determinant of the hA_3AR interaction. In fact, while shorter spacers (e.g. compounds **4-6**) gave good results in terms of both affinity (Ki hA_3 = 2.75-4.47 nM) and selectivity (hA_{2A}/hA_3 = 54.5-88) for the hA_3AR (e.g. compound **3**, Ki hA_3 = 2.75 nM, hA_1/hA_3 = > 3,636; hA_{2A}/hA_3 = 54.5), longer diamino moieties (e.g compounds **7, 8**) led to derivatives showing a significant loss of affinity at the hA_3AR with a consequent reduction of selectivity, especially towards the $hA_{2A}AR$ subtype (e.g. compound **8**, Ki hA_3 = 82.4 nM, hA_1/hA_3 > 133; hA_{2A}/hA_3 = 6.1).

However, the corresponding *N*-BOC deprotected derivatives **9-13** showed good hA_3AR affinity independently of the spacer length, albeit, in general, the selectivity vs the $hA_{2A}AR$ subtype was significantly reduced with respect to the *N*-BOC derivatives (**4-8**) (e.g. compound **10**, Ki hA_3 = 6 nM, hA_1/hA_3 = > 1,666; hA_{2A}/hA_3 = 28 vs. compound **5**, Ki hA_3 = 3.46 nM, hA_1/hA_3 = > 2,890; hA_{2A}/hA_3 = 88). Interestingly, compounds bearing PEG-like spacers (**7**, **8** and **12**, **13**) showed a different selectivity profile, denoting that also the nature of the spacer was important for the AR interactions, in particular for the hA_{2A} and hA_3 ARs. In fact, while in the BOC protected series a very low selectivity was observed (compound **7**, hA_{2A}/hA_3 = 6.1 and compound **8**, hA_{2A}/hA_3 = 3.9), in the free amino series, compounds gained affinity and selectivity towards the hA_3AR subtype (compound **12**, hA_{2A}/hA_3 = 14 and compound **13**, hA_{2A}/hA_3 = 30.3). In order to assess if the nature, and in particular the polarity of the linker could be someway related to the affinity profile displayed by compounds, the logarithm of the octanol/water partition coefficient ($\log P_{(o/w)}$) was calculated for each compound (Figure 3). As expected, Boc-*free* ligands showed lower values than Boc-functionalized ones, with polyethers being more polar than alkyls. Only for the Boc-free mini-series, the affinity at the hA_3AR increased with the $\log P_{(o/w)}$ value of the compound, while in the other homologous series a correlation between polarity and affinity at the three adenosine receptors was not observed.

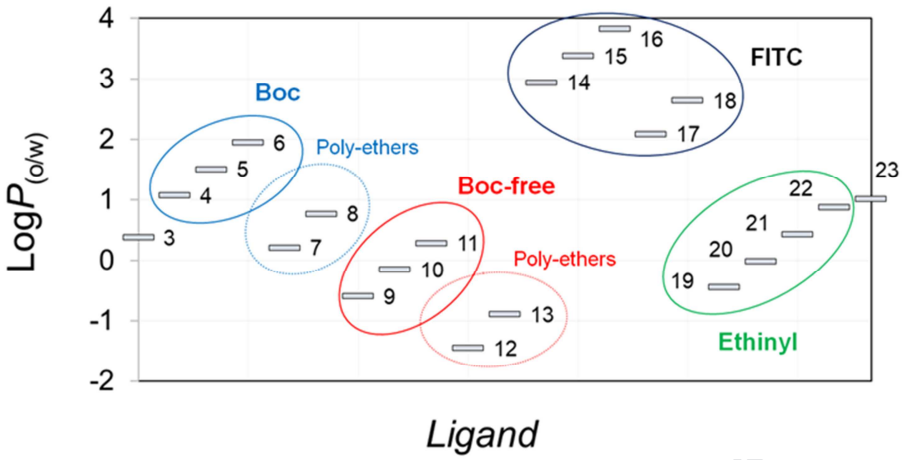

Figure 3. Calculated octanol/water partition coefficient logarithm.

Concerning the fluorescent ligands, introduction of a fluorophore such as FITC on amino function gave compounds **14-18** which showed a significant reduced hA_3AR affinity with a drastic reduction of selectivity vs $hA_{2A}AR$, independently of the spacer length. (e.g. compound **16**, Ki hA_3 = 96.7 nM, hA_1/hA_3 = > 103; hA_{2A}/hA_3 = 1.1). Thus, they can be considered as dual hA_{2A}/hA_3AR fluorescent ligands.

In the amido alkynyl series (**19-22**), all the synthesized compounds proved to be quite potent at the hA_3AR with affinity ranging from 4 to 12 nM and poor affinities versus the other AR subtypes, even if the $hA_{2A}AR$ selectivity was not pronounced (e.g. compound **21**, Ki hA_3 = 7.26 nM, hA_1/hA_3 = 122; hA_{2A}/hA_3 = 20.7). These results suggest that the triple bond likely formed interactions with nonconserved residues in the hA_3AR binding site.

Finally, Alexa Fluor-488 conjugated derivative **23**, a potential fluorescent ligand, retained a good affinity at the hA_3AR (Ki hA_3 = 31.8 nM) and selectivity towards the $hA_{2A}AR$ was improved (hA_1/hA_3 = 2.83) compared to FITC derivatives (**19-22**), even if further optimization is needed (Table 1).

It is quite clear that, in the present case, it was not possible to obtain a conjugable, selective ligand which could be differentially functionalized and that retained the selectivity and affinity profile of the parent compound. Even if the functional moiety (such as the fluorophore), was separated from the pharmacophore through a long spacer, it influenced the ligand-receptor recognition process.

Molecular modelling studies were performed with a view to rationalize affinity data and SAR of the tested ligands. Molecular docking simulations were performed on each AR subtype, using inactive states, in the presence of the sodium ion and its hydration shell [44].

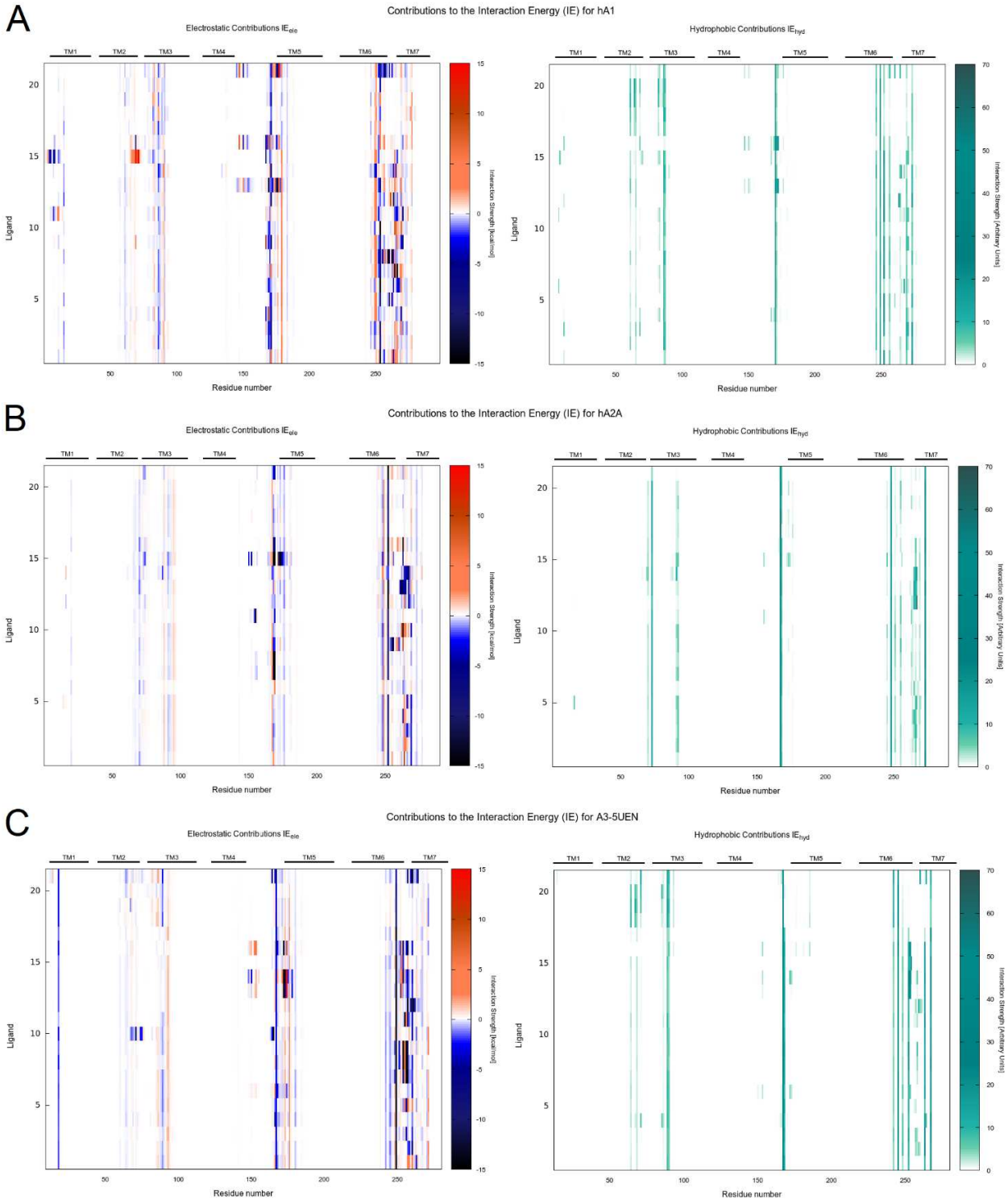

Figure 4. IE map of the electrostatic and hydrophobic interactions between each compound (y-axis) and each residue (x-axis) of AR subtypes (hA_1, A; hA_{2A}, B; hA_3, C) The strength of the electrostatic interaction is represented by a colorimetric scale going from blue to red, from negative to positive values. The strength of the hydrophobic interaction is represented by a colorimetric scale going from white to dark green, from low to high values.

Independently of the receptor subtype considered, the ligands retained the classical binding pattern of

AR antagonists: hydrogen bonds with Asn (6.55) and π-π interactions with Phe (EL2) (Videos S1-3). Moreover, the linker was generally oriented towards the ELs. Despite the overall findings, in the case of the hA_1AR (Video S1), several binding modes result energetically unfavorable or geometrically unreliable (e.g. pointing the furyl ring towards the ELs), consistent with the high A_3AR selectivity observed vs A_1. Interaction energy fingerprint (IEF) maps calculated for each docking pose on three subtypes, revealed that docking at the hA_1AR (Figure 4, A) was less favorable than at hA_{2A} and hA_3 ARs (Figure 4, B-C), because of unfavorable electrostatics at the EL2 and TMs 5-7. hA_3AR ligand poses were highly favored at these locations, more than at hA_{2A} and hA_1 ARs, also in terms of hydrophobic contacts. Furthermore, as explained below, in the hA_3AR, TM1 contributed significantly to stabilization by electrostatics, differently from other subtypes.

Per-residue interaction energy profiles (electrostatic, van der Waals and hydrophobic contributions) were calculated for three representative antagonists: **3** (EA2), **16** (FITC ligand, EA8) and **22** (ethynyl ligand, EA20). Both conserved and non-conserved residues for each receptor subtype were chosen from TMs and ELs, in order to give a better understanding of how they affect binding affinity and selectivity, as shown in Figures 5-7.

Antagonist **3** (EA2) is the parent compound of the series. Nonetheless, it is the only one to show affinity towards the $hA_{2A}AR$ in the micromolar range (Ki hA_{2A} = 1.01 μM, Ki hA_3 = 128 nM). Interestingly, it is characterized by a negatively charged carboxylic moiety. When docked to the hA_1AR, the ligand pose is highly disfavoured by strong repulsion with Glu172 (EL2) and other polar residues (Figure 5). Similarly, at the $hA_{2A}AR$, Glu169 (EL2) disfavors the final state. The mutation of Glu into Val169 at the EL2, and the mutation of Val in Leu90 (3.32) at the TM3 of the hA_3AR are crucial in improving complex stability by hydrophobic interactions. These results predict that negatively charged moieties, exposed to the ELs of the hA_1 and hA_{2A} ARs, inhibit binding by electrostatic repulsion with Glu (EL2). Finally, a favourable electrostatic interaction is observed with the conserved residue Glu19 (1.39) at the TM1 of the hA_3AR, while the same is absent in other subtypes, giving indications about the different shape and nature of the A_3 binding site. The antagonist **16** (EA8, Figures 6 and 7), bearing a longer linker and a fluorophore moiety (FITC), shows strong van der Waals repulsion with Glu172 (EL2) and Asn254 (6.55) at the hA_1AR, while such interactions are favourable at the hA_2AR (Glu169, Asn253) and accompanied by several hydrophobic contacts (Leu267 (6.70), Val92 (3.32), Ile74 (3.14)). The hA_3AR shows a similar profile, but hydrophobic interactions are not significant, consistently with the absence of selectivity observed, as compared to A_{2A}. However, nonconserved residues Gly257, Glu258 and Gln261 (EL3) contribute favourably by electrostatic and van der Waals interactions with the phenyl-acetamido moiety at the 5 position of the PTP. The FITC moiety is also involved and

interacts with several residues located at the ELs 2 and 3, participating in the overall recognition process. As shown in Figure 7, the alkyl linker sits between the loops and adapts to their conformation thanks to its high rotational fredoom. Depending on the latter, the fluorophore is pointed between the ELs, facing several polar residues like Thr173, Arg174 (EL2) and Asn256 (EL3).

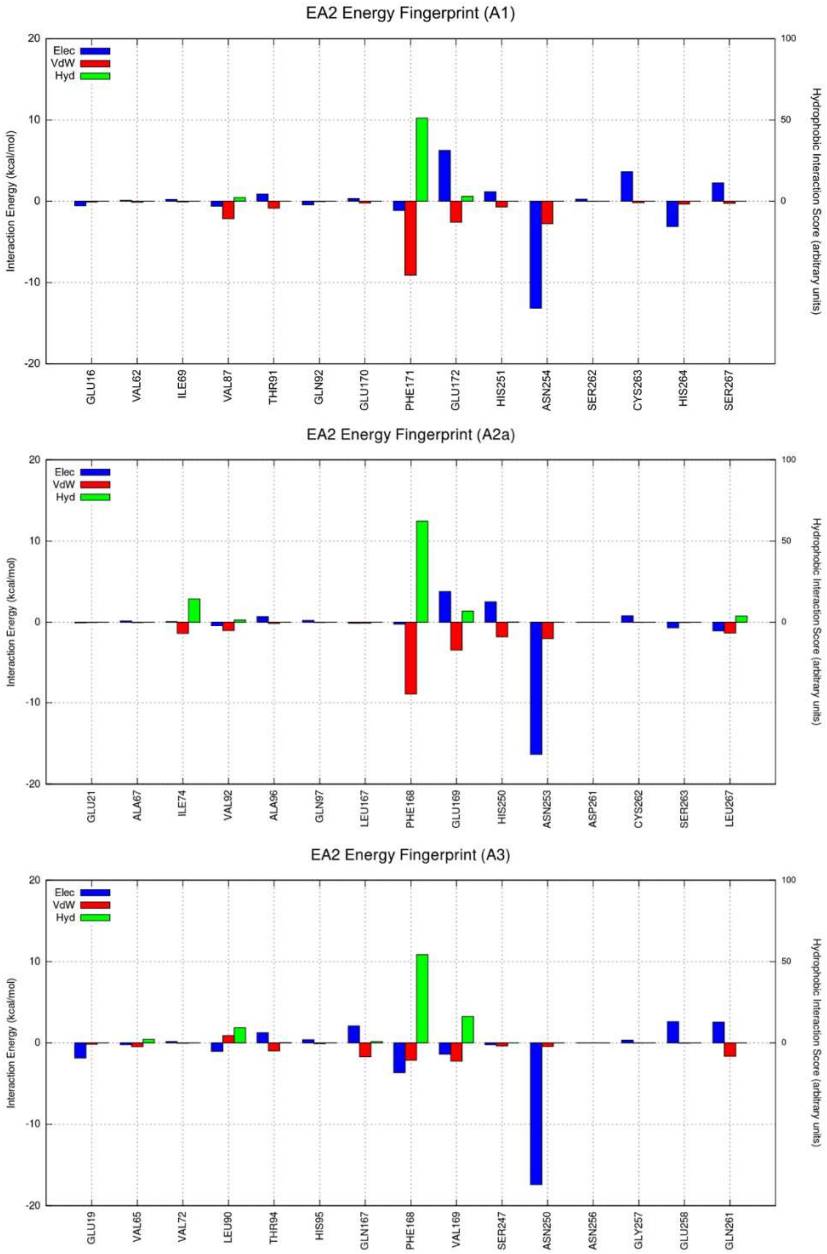

Figure 5. Interaction energy histograms of compound **3** (EA2) for conserved and non-conserved residues of A_1, A_{2A} and A_3 subtypes.

Ethynyl derivative **22** (EA20) prefers the hA_3AR cavity through several hydrophobic contacts with non-conserved residues and electrostatic interactions, mainly due to the terminal triple bond, which could explain the selectivity observed (Figure 8). At the $hA_{2A}AR$, in fact, such interactions are absent,

and even some electrostatic repulsion is observed with Glu169 (EL2) and His250 (6.52).

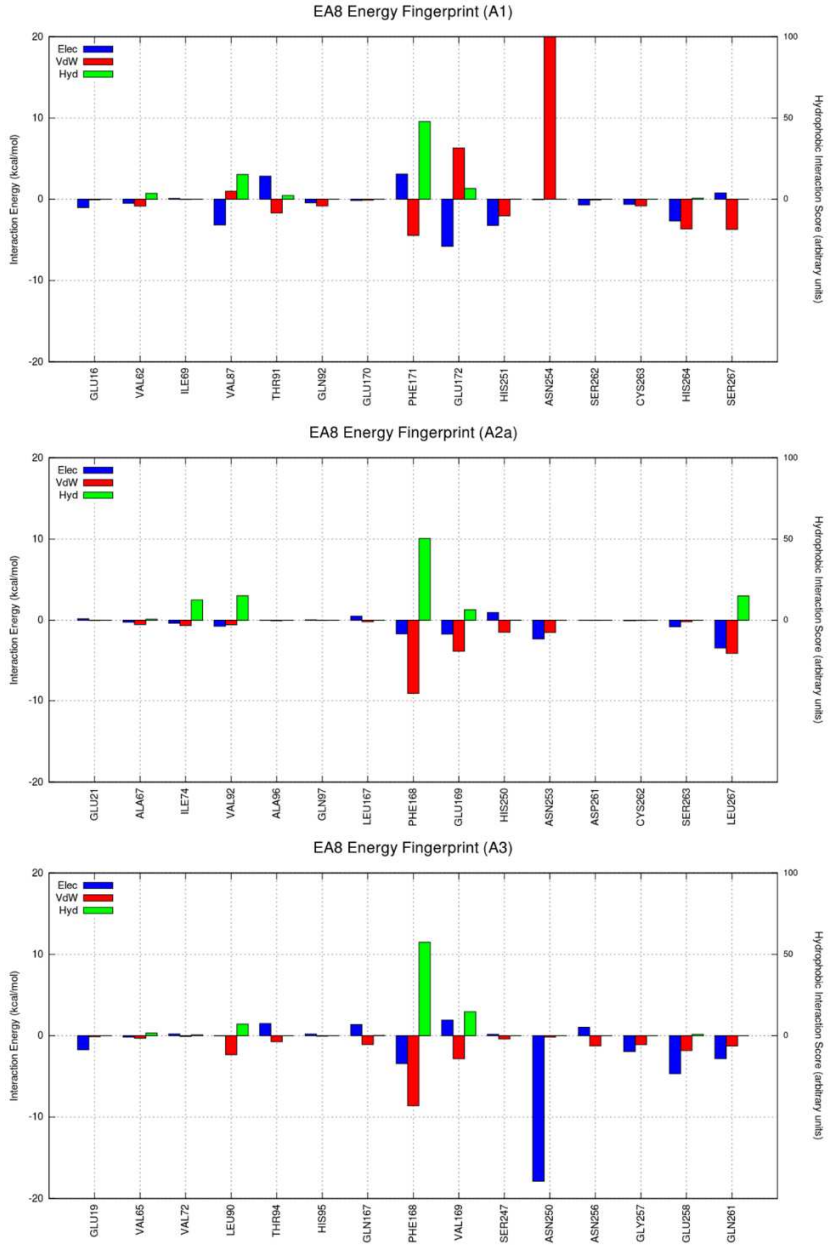

Figure 6. Interaction energy histograms of compound **16** (EA8) for conserved and non-conserved residues of A_1, A_{2A} and A_3 subtypes.

Finally, three supervised molecular dynamics (SuMD) simulations were performed with a view to 1) simulate binding to the hA_3AR, 2) inspect which structural domains at the extracellular side or the hydrophobic cavity may be determinants of the ligand preference. Ligand **3** (EA2) was chosen because it yields the lowest affinity towards the $hA_{2A}AR$ within the entire series while preserving affinity for the A_3 subtype in the nanomolar range. Moreover, basing on per-residue interaction fingerprints (Figures 5-6-8), its carboxylic moiety is clearly important for the A_{2A}/A_3 selectivity. The ligand completely reached the binding site only in simulation 1. As shown in Video S4, the ligand intercalates between the ELs 2-3 and

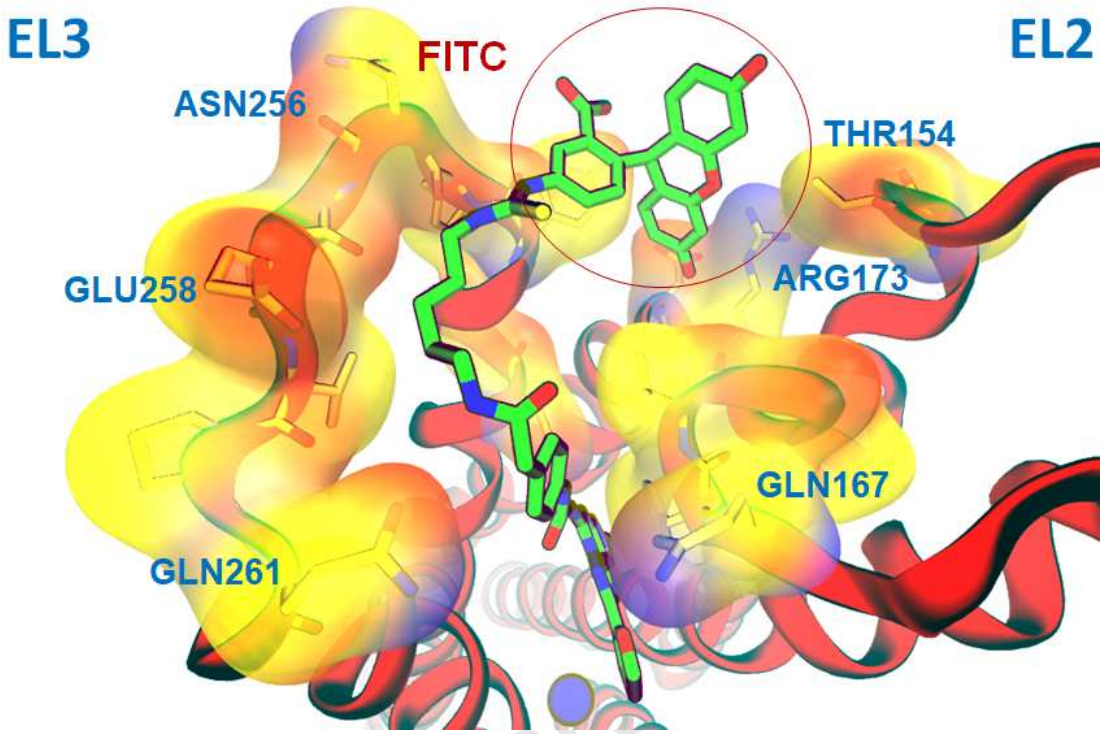

Figure 7. Selected docking pose of ligand 16 (EA8) at the hA_3AR subtype and visualization of the most relevant structural regions interacting with the linker and the fluorophore (FITC).

finally binds the receptor assuming a pose closely resembling the one predicted by molecular docking (Video S1). Two residues (conserved and non-conserved, respectively) seem to play an important role in the recognition process: Glu19 (1.39) and Gln261 (EL3). Glu19, located at the TM1, interacts with the pyrazole ring favouring binding during the entire process. Gln261 (EL3) (Leu267 in the hA_{2A} AR) makes hydrogen bonds with the ligand's carboxylate exposed to the ELs, either in the initial phase of approach or in the phase of stabilization. Such interaction is detectable in the ligand-protein interaction energy profile for distances of about 10 Å. Interestingly, in both simulations 2 and 3, the ligand stops just at 10 Å, between the ELs 2-3, giving the same interaction energy peak observed in simulation 1 (Figure 9). The interaction energy is weaker than the bound state 1, indicating that the ligand can effectively cross that "barrier". This result indicates that the ELs' structural region is crucial for binding, as ligands can cross it more (or less) efficiently depending on the specific substitution present at the 5 position of PTP. Indeed, the ligand **3** establishes highly favorable contacts even at long distances, corresponding to the EL3 or EL2 (20-30 Å), where several non-conserved residues are located, in agreement with per-residue interaction energy calculations. Some contacts are more stabilizing than the final state 1 (meta-binding sites), however, the great conformational freedom of the EL2 (see Video S4) could explain the progression of the ligand path.

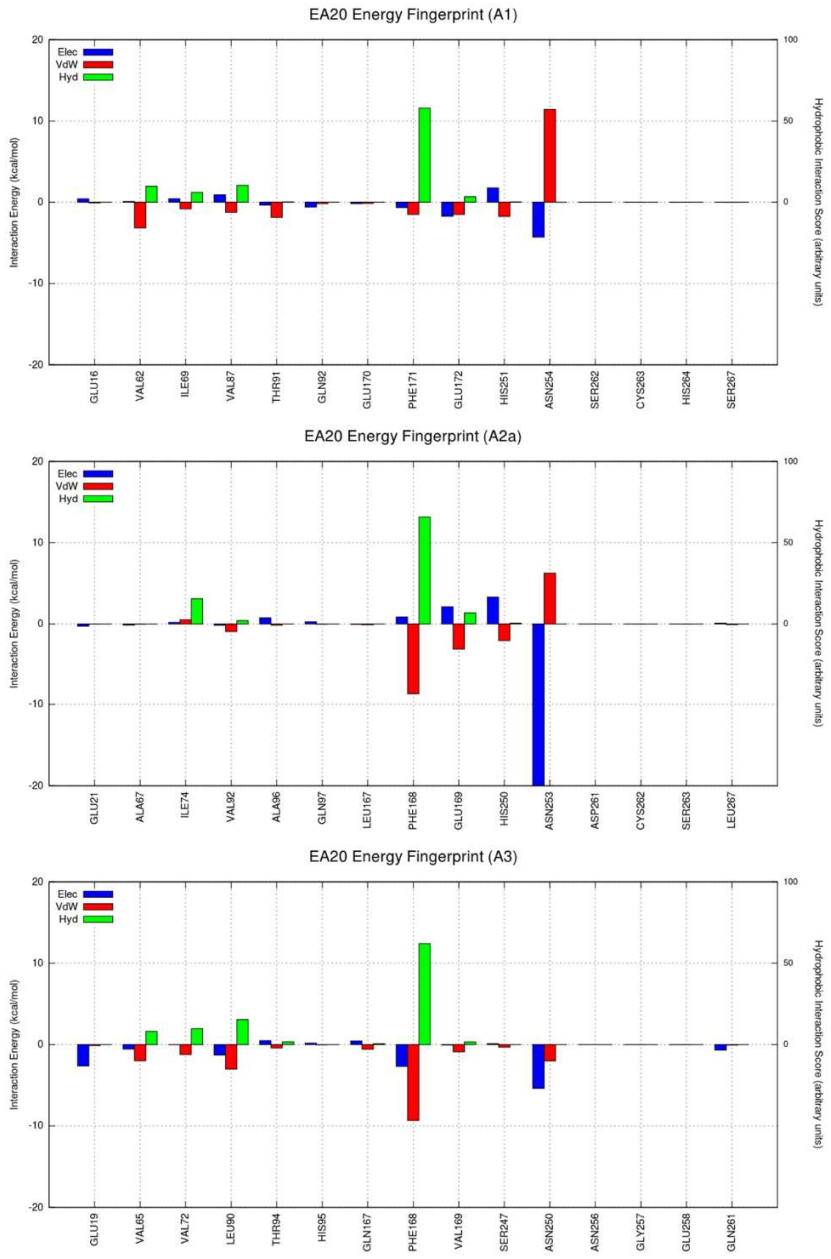

Figure 8. Interaction energy histograms of compound 22 (EA20) for conserved and non-conserved residues of A_1, A_{2A} and A_3 subtypes.

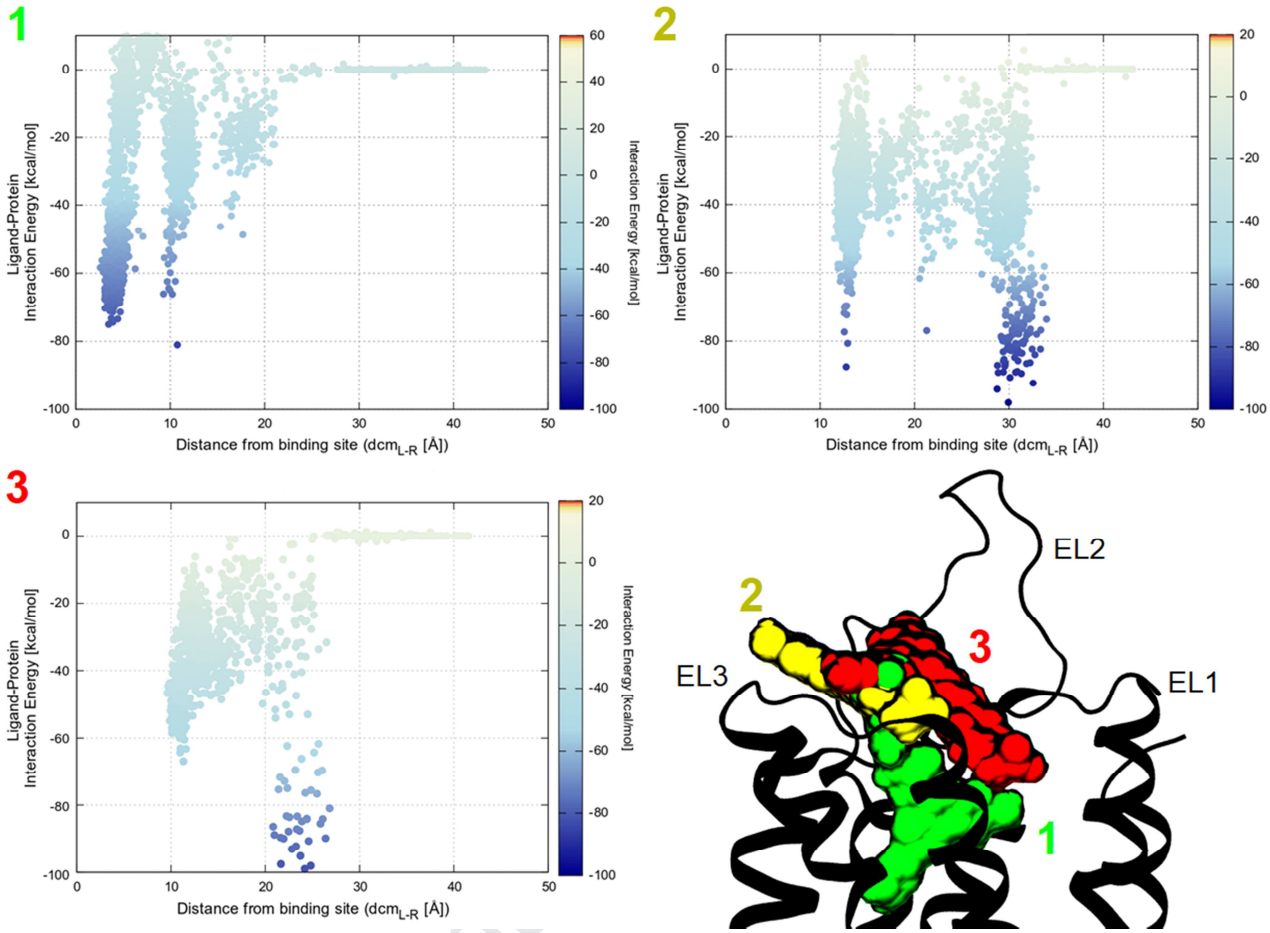

Figure 9. Ligand **3** (EA2)-protein interaction energy vs distance from the binding site, for each SuMD simulation. VdW surfaces of the respective final states are reported with different colors, along with particular regions of the receptor.

Experimental Section

Chemistry

General. Reactions were routinely monitored by thin-layer chromatography (TLC) on silica gel (precoated Macherey-Nagel, 60FUV254). Flash chromatography was performed using Macherey-Nagel, silica 60, 230-400 mesh silica gel. Light petroleum ether refers to the fractions boiling at 40-60 °C. Melting points were determined on a Buchi-Tottoli instrument and are uncorrected. ^{1}H-NMR were determined in $CDCl_3$, DMSO-d_6 or CD_3OD solutions with a Varian Gemini 200, a Bruker 400 or a Varian 500 spectrometers. Peaks positions are given in parts per million (δ) downfield relative to the central peak of the solvents, and J values are given in Hz. The following abbreviations were used: s, singlet; bs, broad singlet; d, doublet; dd, double doublet; bd, broad doublet; t, triplet; m, multiplet. Electrospray mass spectra were recorded on a ESI Bruker 4000 Esquire spectrometer and compounds were dissolved in methanol; accurate mass spectra were recorded on a micrOTOF-Q-Bruker and compounds were dissolved in methanol. Absorption experiments were performed on a Varian Cary

5000 spectrophotometer. Fluorescence measurements were recorded on Varian Cary Eclipse fluorescence spectrophotometer, with excitation filter at 361 nm, emission filter at 390-600 nm (all experiments were performed using a λ_{ex} of 488 nm). Oct-7-ynoic acid was synthesized as reported in the literature.

Synthesis of 2-(4-(3-(2-(furan-2-yl)-8-methyl-8*H*-pyrazolo[4,3-*e*][1,2,4]triazolo[1,5-*c*]pyrimidin-5-yl)ureido)phenyl)acetic acid (3). Ethyl ester derivative **24** (1.95 mmol, 900 mg) was dissolved in a mixture of tetrahydrofuran/methanol/water (4:1:1, 12 mL) and lithium hydroxide monohydrate (5.9 mmol, 245 mg) was added. The suspension was stirred at room temperature overnight. Reaction was monitored by TLC (ethyl acetate 9.5 / methanol 0.5). Water was added to the mixture, the solution was cooled to 0°C and 1 M hydrochloric acid was added (pH 2) leading to the precipitation of a pale brown solid. Solid was filtered and washed with ethyl ether and identified as the desired compound in a quantitative yield. Mp >300°C; ^{1}H-NMR (200 MHz, DMSO-d_6) δ 10.67 (s, 1H) 9.55 (bs, 1H), 8.78 (s, 1H), 7.93 (s, 1H) 7.78-7.36 (m, 3H), 7.38–6.96 (m, 3H), 6.76 (bs, 1H), 4.34 (s, 3H), 3.56 (s, 2H). ES-MS negative mode (methanol) m/z: 431.0 $[M-H]^-$.

General procedure for the synthesis of amides 4-8. The carboxylic acid derivative **3** (0.58 mmol, 250 mg) was dissolved in DMF (3 mL) and the appropriate mono-BOC-protected diamine (**25-29**) was added (0.58 mmol). Reaction was stirred and cooled to 0°C under an argon atmosphere and then 1-ethyl-3-(3-dimethylaminopropyl)carbodiimmide hydrochloride (EDCI·HCl, 1.16 mmol, 222 mg) and 4-dimethylaminopyridine (DMAP, 1.44 mmol, 177 mg) were added. Mixture was stirred at room temperature overnight and monitored by TLC (dichloromethane 9.3 / methanol 0.7). The solvent was evaporated under reduced pressure. The residue was suspended in water and extracted with ethyl acetate (3 times). The organic layers were collected and dried over sodium sulfate anhydrous and the solvent removed under reduced pressure. The crude product was purified on flash silica column chromatography (dichloromethane 9.7 / methanol 0.3) to afford the desired compound (**4-8**).

***tert*-Butyl (3-(2-(4-(3-(2-(furan-2-yl)-8-methyl-8*H*-pyrazolo[4,3-*e*][1,2,4]triazolo[1,5-*c*]pyrimidin-5-yl)ureido)phenyl)acetamido)propyl)carbamate (4).** Yield 29.4%; white solid; mp 198-205°C; ^{1}H-NMR (200 MHz, $CDCl_3$) δ 11.19 (s, 1H), 8.60 (s, 1H), 8.23 (s, 1H), 7.80–7.46 (m, 3H), 7.30–7.26 (m, 3H), 6.62 (dd, J = 3.4, 1.8 Hz, 1H), 6.05 (bs, 1H), 4.94 (bs, 1H), 4.21 (s, 3H), 3.58 (s, 2H), 3.27 (q, J = 6 Hz, 2H), 3.15-3.00 (m, 2H), 1.56 (t, J = 6, 2H), 1.42 (s, 9H); ES-MS (methanol) m/z: 611.3 $[M+Na]^+$. HRMS (ESI-TOF) m/z: $[M+Na]^+$ Calcd for $C_{28}H_{32}N_{10}O_5$ 611.2449; Found 611.2440.

***tert*-Butyl (4-(2-(4-(3-(2-(furan-2-yl)-8-methyl-8*H*-pyrazolo[4,3-e][1,2,4]triazolo[1,5-*c*]pyrimidin-5-yl)ureido)phenyl)acetamido)butyl)carbamate (5).** Yield 34.5%; white solid; mp 186-193°C; ^{1}H-

NMR (200 MHz, $CDCl_3$) δ 11.19 (s, 1H), 8.60 (s, 1H), 8.22 (s, 1H), 7.90–7.48 (m, 3H), 7.38–7.09 (m, 3H), 6.62 (s, 1H), 5.63 (bs, 1H), 4.60 (bs, 1H), 4.21 (s, 3H), 3.57 (s, 2H), 3.22 (bs, 2H), 3.09 (bs, 2H), 1.75 (bs, 4H), 1.43 (s, 9H); ES-MS (methanol) m/z: 625.4 $[M+Na]^+$, 641.3 $[M+K]^+$. HRMS (ESI-TOF) m/z: $[M+Na]^+$ Calcd for $C_{29}H_{34}N_{10}O_5$ 625.2606; Found 625.2608.

***tert*-Butyl (5-(2-(4-(3-(2-(furan-2-yl)-8-methyl-8*H*-pyrazolo[4,3-*e*][1,2,4]triazolo[1,5-*c*]pyrimidin-5-yl)ureido)phenyl)acetamido)pentyl)carbamate (6).** Yield 28%; white solid; mp 78-185°C; ^{1}H-NMR (200 MHz, $CDCl_3$) δ 11.20 (s, 1H), 8.61 (s, 1H), 8.23 (s, 1H), 7.66 (bs, 3H), 7.26 (bs, 3H), 6.62 (bs, 1H), 5.47 (bs, 1H), 4.56 (bs, 1H), 4.21 (s, 3H), 3.57 (s, 2H), 3.20 (bs, 2H), 3.07 (bs, 2H), 1.60-1.10 (m, 15H); ESMS (methanol) m/z: 639.4 $[M+Na]^+$, 655.3 $[M+K]^+$. HRMS (ESI-TOF) m/z: $[M+Na]^+$ Calcd for $C_{30}H_{36}N_{10}O_5$ 639.2762; Found 639.2764.

***tert*-Butyl (2-(2-(2-(2-(4-(3-(2-(furan-2-yl)-8-methyl-8*H*-pyrazolo[4,3-*e*][1,2,4]triazolo[1,5-*c*]pyrimidin-5-yl)ureido)phenyl)acetamido)ethoxy)ethoxy)ethyl)carbamate (7).** Yield 54%; white solid; mp 157-165°C; ^{1}H-NMR (200 MHz, $CDCl_3$) δ 11.18 (s, 1H), 8.60 (s, 1H), 8.23 (s, 1H), 7.78–7.56 (m, 3H), 7.42–7.15 (m, 3H), 6.62 (dd, J = 3.2, 1.6 Hz, 1H), 5.97 (bs, 1H), 5.02 (bs, 1H), 4.22 (s, 3H), 3.73 – 3.35 (m, 12H), 3.29 (bs, 2H), 1.42 (s, 9H); ES-MS (methanol) m/z: 685.4 $[M+Na]^+$, 701.4 $[M+K]^+$. HRMS (ESI-TOF) m/z: $[M+Na]^+$ Calcd for $C_{31}H_{38}N_{10}O_7$ 685.2817; Found 685.2807.

***tert*-Butyl (1-(4-(3-(2-(furan-2-yl)-8-methyl-8*H*-pyrazolo[4,3-*e*][1,2,4]triazolo[1,5-*c*]pyrimidin-5-yl)ureido)phenyl)-2-oxo-7,10,13-trioxa-3-azahexadecan-16-yl)carbamate (8).** Yield 21.6%; white solid; mp 151-158°C; ^{1}H-NMR (270 MHz, $CDCl_3$) δ 11.19 (s, 1H), 8.60 (s, 1H), 8.24 (s, 1H), 7.80–7.61 (m, 3H), 7.45–7.19 (m, 3H), 6.63 (bs, 1H), 6.20 (bs, 1H), 4.96 (bs, 1H), 4.22 (s, 3H), 3.71–3.49 (m, 14H), 3.35 (bs, 2H), 3.20 (bs, 2H), 1.73 (t, J = 3.2, 4H), 1.49 (s, 9H); ES-MS (methanol) m/z: 757.4 $[M+Na]^+$. HRMS (ESI-TOF) m/z: $[M+Na]^+$ Calcd for $C_{35}H_{46}N_{10}O_8$ 757.3392; Found 757.3393.

General synthesis of compounds 9-13 by N-BOC deprotection. The N-BOC protected derivatives (**4-8**) were dissolved in a solution of TFA and dichloromethane (1:1) and the mixtures were stirred for 2 hours at room temperature. Reactions were monitored by TLC (dichloromethane 9.3 / methanol 0.7). The solvent was removed under reduced pressure and the solids were filtered to afford the desired compounds as trifluoroacetate salts (**9-13**).

***N*-(3-aminopropyl)-2-(4-(3-(2-(furan-2-yl)-8-methyl-8*H*-pyrazolo[4,3-*e*][1,2,4]triazolo[1,5-*c*]pyrimidin-5-yl)ureido)phenyl)acetamide trifluoroacetate salt (9).** Yield 89.8%; white solid; mp 142-150°C; ^{1}H-NMR (200 MHz, CD_3OD) δ 11.28 (s, 1H), 8.48 (s, 1H), 8.31 (bs, 1H), 7.76 (s, 1H), 7.62 (d, J = 8.2 Hz, 2H), 7.30 (d, J = 8.2 Hz, 1H), 7.24 (d, J = 3.4 Hz, 1H) 6.66 (bs, 1H), 4.15 (s, 3H), 3.52 (s, 2H), 3.34–3.10 (m, 2H), 2.89 (t, J = 7.0 Hz, 2H), 1.85 (p, J = 7.0 Hz, 2H). HRMS (ESI-TOF) m/z: $[M+H]^+$ Calcd for $C_{23}H_{24}N_{10}O_3$ 489.2106; Found 489.2104.

***N*-(4-aminobutyl)-2-(4-(3-(2-(furan-2-yl)-8-methyl-8*H*-pyrazolo[4,3-*e*][1,2,4]triazolo[1,5-*c*]pyrimidin-5-yl)ureido)phenyl)acetamide trifluoroacetate salt (10).** Yield 95.1%; white solid; mp 167-173°C; ^{1}H-NMR (200 MHz, CD_3OD) δ 8.48 (s, 1H), 8.19 (bs, 1H), 7.76 (s, 1H), 7.63 (d, J = 8.2 Hz, 2H), 7.39–7.13 (m, 3H), 6.70-6.62 (m, J = 1H), 4.14 (s, 3H), 3.51 (s, 2H), 3.32–3.30 (m, 2H), 2.92 (t, J = 6.7 Hz, 2H), 1.78–1.49 (m, 4H). HRMS (ESI-TOF) m/z: $[M+H]^+$ Calcd for $C_{24}H_{26}N_{10}O_3$ 503.2262; Found 503.2260.

***N*-(5-aminopentyl)-2-(4-(3-(2-(furan-2-yl)-8-methyl-8*H*-pyrazolo[4,3-*e*][1,2,4]triazolo[1,5-*c*]pyrimidin-5-yl)ureido)phenyl)acetamide trifluoroacetate salt (11).** Yield 85.3%; white solid; mp 170-178°C; ^{1}H-NMR (200 MHz, CD_3OD) δ 8.47 (s, 1H), 8.13 (bs, 1H), 7.75 (s, 1H), 7.61 (d, J = 7.7 Hz, 2H), 7.29 (d, J = 7.7 Hz, 2H), 7.25 (s, 1H), 6.66 (s, 1H), 4.14 (s, 3H), 3.49 (s, 2H), 3.33–3.08 (m, 2H), 2.88 (t, J = 7.3 Hz, 2H), 1.77–1.47 (m, 4H), 1.47–1.25 (m, 2H). HRMS (ESI-TOF) m/z: $[M+H]^+$ Calcd for $C_{25}H_{28}N_{10}O_3$ 517.2419; Found 517.2417.

2-(2-(2-(2-(4-(3-(2-(furan-2-yl)-8-methyl-8*H*-pyrazolo[4,3-*e*][1,2,4]triazolo[1,5-*c*]pyrimidin-5-yl)ureido)phenyl)acetamido)ethoxy)ethoxy)ethanamine trifluoroacetate salt (12). Yield 83.3%; white solid; mp 152-160°C; ^{1}H-NMR (200 MHz, CD_3OD) δ 8.49 (s, 1H), 8.15 (bs, 1H), 7.76 (bs, 1H), 7.62 (d, J = 7.3 Hz, 2H), 7.44–7.13 (m, 3H), 6.66 (bs, 1H), 4.15 (s, 3H), 3.85–3.38 (m, 12H), 3.09 (bs, 2H); ES-MS (methanol) m/z: 563.3 $[M+H]^+$, 585.3 $[M+Na]^+$. HRMS (ESI-TOF) m/z: $[M+H]^+$ Calcd for $C_{26}H_{30}N_{10}O_5$ 563.2473; Found 563.2474.

***N*-(3-(2-(2-(3-aminopropoxy)ethoxy)ethoxy)propyl)-2-(4-(3-(2-(furan-2-yl)-8-methyl-8*H*-pyrazolo[4,3-*e*][1,2,4]triazolo[1,5-*c*]pyrimidin-5-yl)ureido)phenyl)acetamide trifluoroacetate salt (13).** Yield 94.2%; white solid; mp 133-140°C; ^{1}H-NMR (270 MHz, $CDCl_3$) δ 11.13 (s, 1H), 8.28 (s, 1H), 7.81 (bs, 2H), 7.66 (s, 1H), 7.60 (d, J = 7.7 Hz, 2H), 7.41–7.13 (m, 3H), 6.62 (s, 1H), 5.40 (bs, 2H), 4.21 (s, 3H), 3.75 (s, 2H), 3.66–3.54 (m, 12H), 3.36 (bs, 2H), 3.24 (bs, 2H), 2.02 (bs, 2H), 1.78 (bs, 2H). HRMS (ESI-TOF) m/z: $[M+H]^+$ Calcd for $C_{38}H_{38}N_{10}O_6$ 635.3049; Found 635.3046.

General synthesis of fluorescein conjugates (14-18). 0.075 mmol of amino derivatives **9-13** were dissolved in 4 mL of dry methanol. 21.6 µL (0.155 mmol) of TEA were added to the solution which was stirred at room temperature for 30 minutes under an argon atmosphere. Then 30.2 mg (0.075 mmol) of FITC were added and the reaction was stirred for 72 hours in the dark. The products were purified by column chromatography starting with dichloromethane:methanol (9:1) as eluent. The obtained solids were suspended in dichloromethane, filtered and washed several times with ethyl ether yielding to the desired compounds as orange solids (**14-18**).

5-(3-(3-(2-(4-(3-(2-(furan-2-yl)-8-methyl-8*H*-pyrazolo[4,3-*e*][1,2,4]triazolo[1,5-*c*]pyrimidin-5-yl)ureido)phenyl)acetamido)propyl)thioureido)-2-(6-hydroxy-3-oxo-3*H*-xanthen-9-yl)benzoate

(14). Yield 54.7%; orange solid; mp 198-204°C; ^{1}H-NMR (200 MHz, DMSO-d_6) δ 10.69 (s, 1H), 10.09 (bs, 3H), 8.76 (s, 1H), 8.41–8.05 (m, 3H), 7.98 (s, 1H), 7.76 (d, J = 3.2 Hz, 1H), 7.50 (d, J = 7.4 Hz, 2H), 7.39–7.03 (m, 4H), 6.76 (s, 1H), 6.65–6.47 (m, 6H), 4.12 (s, 3H), 3.50 (bs, 2H), 3.35 (s, 2H), 3.15 (bs, 2H), 1.71 (bs, 2H); ^{13}C-NMR (50 MHz, DMSO-d_6) δ 180.29, 170.29, 168.44, 160.06, 159.79, 154.77, 152.93, 151.98, 151.93, 151.91, 149.57, 149.52, 148.96, 148.89, 145.30, 144.99, 141.23, 140.14, 136.60, 131.29, 129.65, 129.59, 129.49, 129.23, 129.20, 129.16, 129.13, 129.01, 126.24, 124.15, 118.95, 112.68, 112.54, 112.18, 109.81, 102.17, 98.68, 45.69, 41.86, 41.44, 36.37, 28.73; UV-VIS λ_{max} 523 nm; Fluorescence λ_{em} 537; ES-MS (methanol) m/z 878.3 $[M+H]^+$, 900.3 $[M+Na]^+$, 916.3 $[M+K]^+$. HRMS (ESI-TOF) m/z: $[M+H]^+$ Calcd for $C_{44}H_{35}N_{11}O_8S$ 878.2464; Found 878.2336.

5-(3-(4-(2-(4-(3-(2-(furan-2-yl)-8-methyl-8*H*-pyrazolo[4,3-*e*][1,2,4]triazolo[1,5-*c*]pyrimidin-5-yl)ureido)phenyl)acetamido)butyl)thioureido)-2-(6-hydroxy-3-oxo-3*H*-xanthen-9-yl)benzoate (15). Yield 53.8%; orange solid; mp 200-207°C; ^{1}H-NMR (200 MHz, DMSO-d_6)δ 10.72 (s, 1H), 10.06 (bs, 3H), 8.74 (s, 1H), 8.26 (bs, 2H), 8.07 (bs, 1H), 7.96 (s, 1H), 7.76 (d, J = 6.9 Hz, 1H), 7.50 (d, J = 8.0 Hz, 2H), 7.35–7.08 (m, 4H), 6.75 (s, 1H), 6.70-6.37 (m, 6H), 5.76 (s, 1H), 4.11 (s, 3H) 3.36 (s, 2H), 3.08 (bs, 4H), 1.51 (bs, 4H); ^{13}C-NMR (50 MHz, DMSO-d_6) δ 180.21, 169.96, 168.47, 160.33, 160.10, 154.46, 153.01, 152.94, 152.43, 152.19, 149.96, 149.86, 148.88, 148.81, 145.30, 145.03, 141.33, 140.40, 136.61, 131.40, 129.44, 129.10, 129.04, 129.02, 126.20, 124.23, 118.98, 112.94, 112.91, 112.45, 112.16, 109.88, 102.25, 98.62, 45.76, 43.43, 41.85, 38.10, 26.82, 25.84; UV-VIS λ_{max} 524 nm; Fluorescence λ_{em} 535; ES-MS (methanol) m/z: 892.4 $[M+H]^+$, 914.3 $[M+Na]^+$, 930.3 $[M+K]^+$. HRMS (ESI-TOF) m/z: $[M+H]^+$ Calcd for $C_{45}H_{37}N_{11}O_8S$ 914.2439; Found 914.2437.

5-(3-(5-(2-(4-(3-(2-(furan-2-yl)-8-methyl-8*H*-pyrazolo[4,3-*e*][1,2,4]triazolo[1,5-*c*]pyrimidin-5-yl)ureido)phenyl)acetamido)pentyl)thioureido)-2-(6-hydroxy-3-oxo-3*H*-xanthen-9-yl)benzoate (16). Yield 28%; orange solid; mp 190-200°C; ^{1}H-NMR (200 MHz, DMSO-d_6) δ 10.73 (s, 1H), 10.13 (bs, 1H), 8.75 (s, 1H), 8.27 (bs, 2H), 8.11–7.87 (m, 2H), 7.76 (d, J = 5.6 Hz, 1H), 7.50 (d, J = 6.3 Hz, 2H), 7.39–7.02 (m, 4H), 6.75 (s, 1H), 6.71–6.39 (m, 6H), 4.12 (s, 3H), 3.38 (s, 2H), 3.07 (bs, 4H), 1.74–1.10 (m, 4H), 1.08–0.75 (m, 2H); ^{13}C-NMR (50 MHz, DMSO-d_6) δ 180.17, 169.90, 168.45, 160.02, 159.91, 154.73, 152.99, 151.96, 149.80, 149.77, 148.92, 148.88, 145.24, 145.03, 141.35, 140.32, 136.63, 131.37, 129.49, 129.44, 129.27, 129.23, 129.02, 129.00, 126.21, 124.08, 119.27, 118.92, 112.94, 112.88, 112.85, 112.46, 112.18, 109.86, 102.17, 98.64, 43.74, 41.84, 40.61, 40.20, 28.79, 28.03, 23.88; UV-VIS λ_{max} 523 nm; Fluorescence λ_{em} 537; ES-MS (methanol) m/z: 928.4 $[M+Na]^+$. HRMS (ESI-TOF) m/z: $[M+H]^+$ Calcd for $C_{46}H_{39}N_{11}O_8S$ 928.2596; Found 928.2596.

5-(3-(2-(2-(2-(2-(4-(3-(2-(furan-2-yl)-8-methyl-8*H*-pyrazolo[4,3-*e*][1,2,4]triazolo[1,5-*c*]pyrimidin-5-yl)ureido)phenyl)acetamido)ethoxy)ethoxy)ethyl)thioureido)-2-(6-hydroxy-3-oxo-3*H*-xanthen-

9-yl)benzoate (17). Yield 54.3%; orange solid; mp 182-185°C; 1H NMR ^{1}H-NMR (200 MHz, DMSO-d_6) δ 10.72 (s, 1H), 10.14 (bs, 3H), 8.75 (s, 1H), 8.30 (s, 1H), 8.13 (d, J = 5.0 Hz, 2H), 7.95 (s, 1H), 7.76 (d, J = 7.7 Hz, 1H), 7.49 (d, J = 7.9 Hz, 2H), 7.37–7.07 (m, 4H), 6.74 (s, 1H), 6.69–6.42 (m, 6H), 4.11 (s, 3H), 3.79–3.48 (m, 8H), 3.51–2.86 (m, 6H); ^{13}C-NMR (50 MHz, DMSO-d_6) δ 180.47, 170.26, 168.54, 159.65, 159.61, 154.82, 154.78, 152.92, 151.96, 151.86, 149.68, 148.89, 145.26, 145.00, 141.27, 140.25, 136.60, 131.30, 129.58, 129.47, 128.97, 126.77, 126.27, 124.04, 118.95, 112.70, 112.67, 112.53, 112.19, 109.77, 102.21, 102.19, 98.68, 69.62, 69.52, 69.07, 68.46, 45.70, 43.69, 41.71, 41.03; UV-VIS λ_{max} 524 nm; Fluorescence λ_{em} 537; ES-MS (methanol) m/z: 952.4 $[M+H]^+$, 974.4 $[M+Na]^+$, 990.4 $[M+K]^+$. HRMS (ESI-TOF) m/z: $[M+H]^+$ Calcd for $C_{47}H_{41}N_{11}O_{10}S$ 952.2831; Found 952.2833.

5-(3-(1-(4-(3-(2-(furan-2-yl)-8-methyl-8*H*-pyrazolo[4,3-*e*][1,2,4]triazolo[1,5-*c*]pyrimidin-5-yl)ureido)phenyl)-2-oxo-7,10,13-trioxa-3-azahexadecan-16-yl)thioureido)-2-(6-hydroxy-3-oxo-3*H*-xanthen-9-yl)benzoate (18). Yield 63%; orange solid; mp 143-149°C; ^{1}H-NMR (200 MHz, DMSO-d_6) δ 10.65 (bs, 1H), 10.36–9.87 (m, 3H), 9.51 (bs, 1H), 8.78 (s, 1H), 8.34–8.11 (m, 2H), 7.99 (s, 2H), 7.74 (d, J = 8.2 Hz, 1H), 7.49 (d, J = 7.8 Hz, 2H), 7.37–7.03 (m, 4H), 6.76 (s, 1H), 6.69–6.45 (m, 6H), 4.13 (s, 3H), 3.65–3.18 (m, 14H), 3.18–2.79 (m, 4H), 1.81 (bs, 2H), 1.63 (bs, 2H); ^{13}C-NMR (50 MHz, DMSO-d_6) δ 180.23, 169.94, 168.39, 159.33, 159.27, 154.82, 151.74, 149.01, 148.96, 148.89, 145.34, 144.91, 141.28, 139.69, 136.40, 131.51, 129.47, 129.38, 129.27, 129.22, 128.92, 128.77, 126.34, 123.87, 118.94, 112.66, 112.49, 112.47, 112.39, 112.21, 112.15, 109.43, 102.16, 98.78, 69.72, 69.53, 69.51, 68.13, 68.01, 41.82, 41.35, 40.62, 35.97, 29.31, 28.58, 9.10; UV-VIS λ_{max} 524 nm; Fluorescence λ_{em} 537; ES-MS (methanol) m/z: 1046.4 $[M+Na]^+$. HRMS (ESI-TOF) m/z: $[M+Na]^+$ Calcd for $C_{51}H_{49}N_{11}O_{11}S$ 1026.3226; Found 1026.3223.

General synthesis for the N-(2-(furan-2-yl)-8-methyl-8H-pyrazolo[4,3-*e*][1,2,4]triazolo[1,5-*c*]pyrimidin-5-yl)alkynamides (19-22). Alkyne acid (1.175 mmol) (**31-24**) was dissolved in deuterated chloroform (2 mL) and a catalytic amount of DMF was added (200 µL). The solution was cooled to 0°C and oxalyl dichloride was added dropwise (1.175 mmol, 99 µL) and the reaction was stirred at room temperature for 3 hours. A little amount of reaction was diluted in deuterated chloroform and monitored by ^{1}H-NMR. The peaks of desired acyl chlorides (**35-38**) were shifted from those of the corresponding carboxylic acids. When the conversion was complete, to the reaction were added 1,4-dioxane (5 mL), triethylamine (1.959 mmol, 273 µL) and the 5-amino-pyrazolo-triazolo-pyrimidine **30** (0.392 mmol, 100 mg). The reaction was stirred at reflux overnight (TLC ethyl acetate 9.5/ methanol 0.5) then the solvent was removed under reduced pressure. The residue was dissolved in water and extracted with dichloromethane (3 times), The organic layers were collected and dried over

sodium sulfate anhydrous and the solvent removed under reduced pressure. The crude was purified on flash silica column chromatography (ethyl acetate 9.8 / methanol 0.2) to afford the desired compound (**19-22**).

***N*-(2-(furan-2-yl)-8-methyl-8*H*-pyrazolo[4,3-*e*][1,2,4]triazolo[1,5-*c*]pyrimidin-5-yl)pent-4-ynamide (19).** Yield 40%; pale brown solid; mp 264-271 °C d; ^{1}H-NMR (200 MHz, $CDCl_3$) δ 9.11 (s, 1H), 8.22 (s, 1H), 7.65 (s, 1H), 7.23 (s, 1H), 6.61 (s, 1H), 4.20 (s, 3H), 3.50 (t, J = 6.8 Hz, 2H), 2.70 (t, J = 6.8 Hz, 2H), 2.01 (s, 2H); ^{13}C-NMR (50 MHz, $CDCl_3$) δ 171.47, 155.68, 153.84, 148.92, 145.09, 144.81, 138.67, 125.55, 111.13, 112.24, 100.04, 82.89, 74.39, 69.33, 41.06, 37.05, 13.86. ES-MS (methanol) m/z: 336.2 $[M+H]^+$, 358.1 $[M+Na]^+$, 374.1 $[M+K]^+$. HRMS (ESI-TOF) m/z: $[M+Na]^+$ Calcd for $C_{16}H_{13}N_7O_2$ 358.1023; Found 358.1021.

***N*-(2-(furan-2-yl)-8-methyl-8*H*-pyrazolo[4,3-*e*][1,2,4]triazolo[1,5-*c*]pyrimidin-5-yl)hex-5-ynamide (20).** Yield 19%; pale yellow solid; mp 210-216 °C d; ^{1}H-NMR (200 MHz, $CDCl_3$) δ 9.05 (s, 1H), 8.21 (s, 1H), 7.65 (s, 1H), 7.26 (s, 1H), 6.62 (s, 1H), 4.21 (s, 3H), 3.26 (t, J = 6.3 Hz, 2H), 2.40 (s, 2H), 2.18 – 1.85 (m, 3H); ^{13}C-NMR (50 MHz, $CDCl_3$) δ 172.67, 156.07, 153.55, 149.05, 145.19, 144.92, 138.68, 124.95, 112.92, 112.16, 100.13, 83.49, 69.33, 40.80, 36.69, 23.34, 18.04. ES-MS (methanol) m/z: 372.2 $[M+Na]^+$. HRMS (ESI-TOF) m/z: $[M+Na]^+$ Calcd for $C_{17}H_{15}N_7O_2$ 372.1179; Found 372.1182.

***N*-(2-(furan-2-yl)-8-methyl-8*H*-pyrazolo[4,3-*e*][1,2,4]triazolo[1,5-*c*]pyrimidin-5-yl)hept-6-ynamide (21).** Yield 15%; white solid; mp 208-215 °C d; ^{1}H-NMR (200 MHz, $CDCl_3$) δ 9.02 (s, 1H), 8.21 (s, 1H), 7.65 (s, 1H), 7.23 (d, J = 3.2 Hz, 1H), 6.60 (d, J = 3.2 Hz 1H), 4.20 (s, 3H), 3.36 (t, J = 7 Hz, 2H), 2.32-2.24 (m, 2H), 1.97-1.86 (m, 3H), 1.77-1.66 (m, 2H); ^{13}C-NMR (50 MHz, $CDCl_3$) δ 173.09, 155.76, 153.92, 148.96, 144.96, 138.75, 125.38, 112.89, 112.19, 100.05, 84.24, 68.76, 41.03, 37.23, 28.01, 23.52, 18.56. ES-MS (methanol) m/z: 364.2 $[M+H]^+$, 386.2 $[M+Na]^+$, 402.1 $[M+K]^+$. HRMS (ESI-TOF) m/z: $[M+Na]^+$ Calcd for $C_{18}H_{17}N_7O_2$ 386.1336; Found 386.1331.

***N*-(2-(furan-2-yl)-8-methyl-8*H*-pyrazolo[4,3-*e*][1,2,4]triazolo[1,5-*c*]pyrimidin-5-yl)oct-7-ynamide (22).** Yield 40%; white solid; mp 204-208 °C d; ^{1}H-NMR (200 MHz, $CDCl_3$) δ 8.99 (s, 1H), 8.21 (s, 1H), 7.65 (d, J = 1.8 Hz, 1H), 7.25 (d, J = 3.2 Hz, 1H), 6.61 (dd, J = 1.8 Hz, J = 3.2 Hz 1H), 4.20 (s, 3H), 3.24 (t, J = 7.2 Hz, 2H), 2.23-2.04 (m, 2H), 1.95-1.73 (m, 3H), 1.61-1.56 (m, 4H); ^{13}C-NMR (50 MHz, $CDCl_3$) δ 173.28, 155.74, 153.95, 148.95, 144.96, 138.76, 125.37, 112.88, 112.18, 100.06, 84.57, 68.4, 41.02, 37.62, 28.47, 28.38, 23.91, 18.48. ES-MS (methanol) m/z: 378.2 $[M+H]^+$, 400.2 $[M+Na]^+$, 416.1 $[M+K]^+$. HRMS (ESI-TOF) m/z: $[M+Na]^+$ Calcd for $C_{19}H_{19}N_7O_2$ 400.1492; Found 400.1488.

Synthesis of 2-(6-amino-3-iminio-4,5-disulfonato-3*H*-zanthen-9-yl)-5-((6-(4-((8-methyl-2-(furan-2-yl)- 8*H*-pyrazolo[4,3-*e*][1,2,4]triazolo[1,5-*c*]pyrimidin-5-yl)amino)-4-oxobutyl)-1*H*-1,2,3-triazol-1-

yl)hexyl)carbamoyl)benzoate (23)

A solution of Alexa Fluor-488 5-carboxamido-(6-azidohexanyl)bis(triethyammonium salt) (0.5 mg, 0.58 μmol, Invitrogen-Life Technologies, Grand Island, N.Y.) in water (200 μl) was added to a solution of alkyne derivative **20** (0.38 mg, 1.1μmol) in DMF (100 μl). A freshly prepared solution of aqueous sodium ascorbate (0.1 M, 8 μl, 5.86 μmol) was added to the reaction mixture followed by the addition of aqueous copper sulfate pentahydrate solution (0.1 M, 2.94 μl, 0.29 μmol): The resulting mixture was stirred overnight at room temperature; 10 mM aqueous solution of triethylammonium acetate buffer (2 ml) was added with constant mixing. The resulting mixture was lyophilized and purified by HPLC with a Luna 5μ RP.C18 semipreparative column (250 x 10 mm: Phenomenex, Torrance, Calif.) under the following conditions: flow rate of 2 ml/min; H_2O-MeCN from 100:0 (v/v) to 0:100 (v/v) in 30 min and isolated at 20.07 min to get the Alexa Fluor-488 conjugate **23** (0.16 mg, 28%) . Analytical purity > 99% by HPLC (retention time **10.13 min**).

Biology

Radioligand Binding to hA_1, hA_{2A} and hA_3 ARs

[^{3}H]R-PIA and [^{125}I]AB-MECA were utilized in radioligand binding assays to membranes prepared from CHO cells expressing recombinant $hA_1$and hA_3 ARs, respectively, as previously described. [40] While, [^{3}H]CGS21680 binding was used at hA_{2A}AR expressed in HEK293 cells. ADA (3 units/mL) was present during the preparation of the membranes, in a preincubation of 30 min at 30 °C, and during the incubation with the radioligands. All non-radioactive compounds were initially dissolved in DMSO and diluted with buffer to the final concentration, where the amount of DMSO never exceeded 2%. Incubations were terminated by rapid filtration over Whatman GF/B filters, using a Brandell cell harvester (Brandell, Gaithersburg, MD). The tubes were rinsed three times with 3 mL of buffer each. At least six different concentrations of competitor, spanning 3 orders of magnitude adjusted appropriately for the IC_{50} of each compound, were used. IC_{50} values, calculated with the nonlinear regression method implemented in Graph-Pad (Prism, San Diego, CA), were converted to Ki values as described. [40,43]

Computational studies

The MOE suite [45] was used for general molecular modeling operations, including log$P_{(o/w)}$ calculations as well. Preliminary computations were carried out on a 12 CPU (Intel® Xeon® CPU E5-1650 3.80 GHz) Linux workstation. SuMD simulations were performed with the ACEMD engine [46] on NVIDIA drivers: NVIDIA GTX 980Ti and NVIDIA GTX 980. The CHARMM36/CHARMM36

general force field (CGenFF) combination was adopted. The GOLD [47] suite (goldscore scoring function) was used as docking program. Ligands' 3D structures were constructed by the MOE-builder tool. Ionization states were predicted using the MOE-protonate 3D tool. Tautomerization and atom hybridization were checked. Structures were minimized by the MMFF94x until the root mean square (RMS) gradient was below 0.05 kcal mol^{-1} A^{-1}. For each ligand, 20 docking simulation runs were performed on each receptor subtype, searching on a sphere of 20 Å radius, centered on the backbone nitrogen of the conserved Asn (6.55). Ligand and protein partial charges were calculated by means of the MMFF94 and AMBER14:EHT [48] force fields, respectively. The hA_{2A} and hA_1AR coordinates were retrieved from the Protein Data Bank [49] using the crystal structures 3PWH [50] and 5UEN [51], respectively. For the hA_3AR a homology model was used, basing on our docking/structural based model assessment [39]. All molecular docking studies have been carried out with a sodium ion and its first hydration shell in all adenosine receptor structures, according to our previous studies [33]. The Ballesteros‑Weinstein [52] numbering system was used sometimes to indicate conserved residues. IE electrostatic and Van der Waals energy contributions to the binding energy were calculated by MOE, along with per residue electrostatic and hydrophobic interactions. Per-residue information was reported in the "Interaction Energy Fingerprints": they are heat maps reporting the strength of the interaction of each residue (x-axis) and each ligand (y-axis) according to a colorimetric scale going from blue to red for negative to positive values in the case of electrostatic contributions and from white to dark green for low to high values for hydrophobic contributions. Interactions of most relevant residues were also reported by histograms, whose height is proportional to the strength of the interaction. All the plots were generated using Gnuplot 4.6 [53], except Figure 3. Molecular graphics were performed with the UCSF Chimera package [54], except Fig. 8, which was obtained using the VMD program (version 1.9.3) [55]. The in-house MMsDocking video maker tool was exploited to produce videos showing the docking poses, per residue hydrophobic and electrostatic contributions for selected residues, experimental binding data, and scoring values. Representations of docking poses were produced using the UCSF Chimera package, 2D depictions were constructed by the cheminformatics toolkit RDKit [56] and the heat maps were obtained by Gnuplot 4.6; in the end, videos were mounted using MEncoder. Ligand 3 force field parameters for MD simulations were initially retrieved from the Paramchem web service and then deeply optimized in concordance with CGenFF, at the MP2/6-31G [57] level of the theory by using Gaussian 09 [58] and RESP partial charges. Systems were embedded in a 1-palmitoyl-2oleyl-sn-glycerol-3-phospho-choline (POPC) lipid bilayer, according to the pre-orientation provided by the Orientations Proteins in Membrane (OPM) database [59] and by using the VMD membrane

builder plugin. Lipids within 0.4 Å from the protein were removed and TIP3P [60] model water molecules were added to solvate the system by means of Solvate1.0 [61]. Charge neutrality of the system was obtained by adding Na^+/Cl^- counterions to a final concentration of 0.154 M. System was equilibrated through a three-step procedure. In the first step, 1500 conjugate-gradient minimization steps were applied in order to reduce the clashes between protein and lipids. Then, a 5 ns long MD simulation was performed in the NPT ensemble, with a positional constraint of 1 kcal mol^{-1} $Å^{-2}$ on ligand, protein, and lipid phosphorus atoms. During the second stage, 10 ns MD simulation in the NPT ensemble was performed constraining all the protein and ligand atoms but leaving the POPC residues free to diffuse in the bilayer. In the last equilibration stage, positional constraints were applied only to the ligand and protein backbone alpha carbons for further 5 ns MD simulation. All the MD simulations were performed using: (1) an integration time step of 2 fs; (2) the Berendsen barostat [62] to maintain the system pressure at 1 atm; (3) the Langevin thermostat [63] to maintain the temperature at 310 K with a low dumping of 1 ps− 1; (4) the M-SHAKE algorithm [64] to constrain the bond lengths involving hydrogen atoms; and (5) a long-range cutoff of 10 Å. According to the SuMD approach [65,66], the timescale needed to reproduce binding is in the range of nanoseconds, instead of hundreds of nanoseconds or microseconds usually necessary with unsupervised MD. Sampling is performed by a tabu-like algorithm to monitor the distance between the centers of mass of the ligand and the binding site during short unbiased MD simulations. SuMD considers the ligand atoms and the atoms of user-defined protein residues to monitor the distance between the centers of mass of the binder and the binding site. A series of 600 ps unbiased MD simulations are performed and after each simulation, the distance points collected at regular intervals are fitted into a linear function. If the resulting slope is negative the next simulation step starts from the last set of coordinates and velocities produced, otherwise the simulation is restarted by randomly assigning the atomic velocities. Short simulations are perpetuated under the supervision until the distance between the ligand and the binding site goes below 5 Å, then, the supervision is disabled and a classical MD simulation is performed. For the orthosteric center of mass, we considered hA_3AR residues Asn250, Phe168, His272, and Ser247. NAMD energy Plugin 1.4 [67] was used to calculate ligand-protein interaction energies.

Conclusions

In this work we reported a new series of hA_3AR conjugable derivatives that exhibited a very good selectivity towards hA_1AR and a discrete selectivity versus the $hA_{2A}AR$. We have developed both amino compounds, which could be functionalized by reactions with carboxylic acids or isothiocyanates, and alkyne derivatives, which are useful precursors for the click reaction. Unfortunately, attempts to

use these compounds to obtain selective functionalized hA_3AR ligands led mainly to dual hA_{2A}/hA_3 AR ligands, revealing that the functional moiety had an active role in the establishment of ligand-receptor interactions. Moreover, molecular docking and SuMD simulations highlighted that non-conservative residues, located at the ELs 2 and 3 (Gln167, Val169, Gln261, Glu258 of the hA_3AR), constitute a specific structural region able to discriminate ligands depending on their chemical and partition properties. These data can, thus, pave the way for a new understanding of selectivity towards ARs, leading finally to the rational design of highly selective ligands. In any case, among the functionalized compounds, Alexa Fluor 488 derivative MRS5763 (**23**) showed the best hA_3A affinity and selectivity profile, which, by further computer-guided optimization, could lead to a selective hA_3AR probe useful as fluorescent tool for this receptor.

Acknowledgments

KAJ thanks the NIDDK Intramural Research Program (ZIADK31117) for support.

Declaration of interest: none.

References

[1] J. Sawynok, Adenosine receptor targets for pain, Neuroscience. 338 (2016) 1–18. doi:10.1016/j.neuroscience.2015.10.031.

[2] A. Guerrero, A_{2A} adenosine receptor agonists and their potential therapeutic applications. An update, Curr. Med. Chem. 25 (2018) 3597–3612. doi:10.2174/0929867325666180313110254.

[3] B. Hocher, Adenosine A_1 receptor antagonists in clinical research and development, Kidney Int. 78 (2010) 438–445. doi:10.1038/ki.2010.204.

[4] B. Cacciari, G. Spalluto, S. Federico, A_{2A} adenosine receptor antagonists as therapeutic candidates: are they still an interesting challenge?, Mini-Reviews Med. Chem. 18 (2018) 1168–1174. doi:10.2174/1389557518666180423113051.

[5] G. Haskó, B. Csóka, Z.H. Németh, E.S. Vizi, P. Pacher, A_{2B} adenosine receptors in immunity and inflammation., Trends Immunol. 30 (2009) 263–70. doi:10.1016/j.it.2009.04.001.

[6] S.L. Cheong, S. Federico, G. Venkatesan, A.L. Mandel, Y.-M. Shao, S. Moro, G. Spalluto, G. Pastorin, The A_3 adenosine receptor as multifaceted therapeutic target: pharmacology, medicinal chemistry, and in silico approaches, Med. Res. Rev. 33 (2013) 235–335. doi:10.1002/med.20254.

[7] B.B. Fredholm, G. Arslan, L. Halldner, B. Kull, G. Schulte, W. Wasserman, Structure and function of adenosine receptors and their genes, Naunyn. Schmiedebergs. Arch. Pharmacol. 362

(2000) 364–374. doi:10.1007/s002100000313.

[8] P.A. Borea, K. Varani, F. Vincenzi, P.G. Baraldi, M.A. Tabrizi, S. Merighi, S. Gessi, The A_3 adenosine receptor: history and perspectives, Pharmacol. Rev. 67 (2014) 74–102. doi:10.1124/pr.113.008540.

[9] S. Moro, Z. Gao, K.A. Jacobson, G. Spalluto, Progress in the pursuit of therapeutic adenosine receptor antagonists, Med. Res. Rev. 26 (2006) 131–159. doi:10.1002/med.20048.

[10] S. Redenti, A. Ciancetta, G. Pastorin, B. Cacciari, S. Moro, G. Spalluto, S. Federico, Pyrazolo[4,3-*e*][1,2,4]triazolo[1,5-*c*]pyrimidines and structurally simplified analogs. Chemistry and sar profile as adenosine receptor antagonists, Curr. Top. Med. Chem. 16 (2016) 3224–3257. doi:10.2174/1568026616666160506145831.

[11] P.G. Baraldi, B. Cacciari, R. Romagnoli, G. Spalluto, K. Klotz, E. Leung, K. Varani, S. Gessi, S. Merighi, P.A. Borea, Pyrazolo[4,3-*e*]-1,2,4-triazolo[1,5-*c*]pyrimidine Derivatives as highly potent and selective human A_3 adenosine receptor antagonists, J. Med. Chem. 42 (1999) 4473–4478. doi:10.1021/jm991114s.

[12] P.G. Baraldi, B. Cacciari, R. Romagnoli, G. Spalluto, S. Moro, K. Klotz, E. Leung, K. Varani, S. Gessi, S. Merighi, P.A. Borea, Pyrazolo[4,3-*e*]1,2,4-triazolo[1,5-*c*]pyrimidine derivatives as highly potent and selective human A_3 adenosine receptor antagonists: influence of the chain at the N8 pyrazole nitrogen, J. Med. Chem. 43 (2000) 4768–4780. doi:10.1021/jm001047y.

[13] P.G. Baraldi, B. Cacciari, S. Moro, G. Spalluto, G. Pastorin, T. Da Ros, K. Klotz, K. Varani, S. Gessi, P.A. Borea, Synthesis, biological activity, and molecular modeling investigation of new pyrazolo[4,3-*e*]-1,2,4-triazolo[1,5-*c*]pyrimidine derivatives as human A_3 adenosine receptor antagonists, J. Med. Chem. 45 (2002) 770–780. doi:10.1021/jm0109614.

[14] A. Maconi, S. Moro, G. Pastorin, T. Da Ros, G. Spalluto, Z.-G. Gao, K.A. Jacobson, P.G. Baraldi, B. Cacciari, K. Varani, P. Andrea Borea, Synthesis, biological properties, and molecular modeling investigation of the first potent, selective, and water-soluble human A_3 adenosine receptor antagonist, J. Med. Chem. 45 (2002) 3579–3582. doi:10.1021/jm020974x.

[15] S. Federico, A. Ciancetta, D. Sabbadin, S. Paoletta, G. Pastorin, B. Cacciari, K.N. Klotz, S. Moro, G. Spalluto, Exploring the directionality of 5-substitutions in a new series of 5-alkylaminopyrazolo[4,3-*e*]1,2,4-triazolo[1,5-*c*]pyrimidine as a strategy to design novel human A3 adenosine receptor antagonists, J. Med. Chem. 55 (2012). doi:10.1021/jm300899q.

[16] G. Pastorin, T. Da Ros, C. Bolcato, C. Montopoli, S. Moro, B. Cacciari, P.G. Baraldi, K. Varani, P.A. Borea, G. Spalluto, Synthesis and biological studies of a new series of 5-heteroarylcarbamoylaminopyrazolo[4,3-*e*]1,2,4-triazolo[1,5-*c*]pyrimidines as human A_3

adenosine receptor antagonists. Influence of the heteroaryl substituent on binding affinity and molecular modeling in, J. Med. Chem. 49 (2006) 1720–9. doi:10.1021/jm051147+.

[17] P.G. Baraldi, B. Cacciari, S. Dionisotti, J. Egan, G. Spalluto, C. Zocchi, Synthesis of the tritium labeled SCH 58261, a new non-xanthine A_{2A} adenosine receptor antagonist, J. Label. Compd. Radiopharm. 38 (1996) 725–732. doi:10.1002/(SICI)1099-1344(199608)38:8<725::AID-JLCR885>3.0.CO;2-G.

[18] J.C. Shryock, S. Snowdy, P.G. Baraldi, B. Cacciari, G. Spalluto, A. Monopoli, E. Ongini, S.P. Baker, L. Belardinelli, A_{2A} -adenosine receptor reserve for coronary vasodilation, Circulation. 98 (1998) 711–718. doi:10.1161/01.CIR.98.7.711.

[19] S. Todde, R.M. Moresco, P. Simonelli, P.G. Baraldi, B. Cacciari, G. Spalluto, K. Varani, A. Monopoli, M. Matarrese, A. Carpinelli, F. Magni, M.G. Kienle, F. Fazio, Design, Radiosynthesis, and biodistribution of a new potent and selective ligand for in vivo imaging of the adenosine A_{2A} receptor system using positron emission tomography, J. Med. Chem. 43 (2000) 4359–4362. doi:10.1021/jm0009843.

[20] P.G. Baraldi, B. Cacciari, R. Romagnoli, K. Varani, S. Merighi, S. Gessi, P.A. Borea, E. Leung, S.L. Hickey, G. Spalluto, Synthesis and preliminary biological evaluation of [^{3}H]-MRE 3008-F20: the first high affinity radioligand antagonist for the human A_3 adenosine receptors, Bioorg. Med. Chem. Lett. 10 (2000) 209–211. doi:10.1016/S0960-894X(99)00674-5.

[21] P.G. Baraldi, B. Cacciari, S. Moro, R. Romagnoli, X. Ji, K.A. Jacobson, S. Gessi, P.A. Borea, G. Spalluto, Fluorosulfonyl- and bis-(β-chloroethyl)amino-phenylamino functionalized pyrazolo[4,3-*e*]1,2,4-triazolo[1,5-*c*]pyrimidine derivatives: irreversible antagonists at the human A_3 adenosine receptor and molecular modeling studies, J. Med. Chem. 44 (2001) 2735–2742. doi:10.1021/jm010818a.

[22] S. Federico, G. Spalluto, Functionalized ligands targeting G protein-coupled adenosine receptors, Future Med. Chem. 11 (2019) 1673–1677. doi:10.4155/fmc-2019-0133.

[23] L.A. Stoddart, L.E. Kilpatrick, S.J. Briddon, S.J. Hill, Probing the pharmacology of G protein-coupled receptors with fluorescent ligands, Neuropharmacology. 98 (2015) 48–57. doi:10.1016/j.neuropharm.2015.04.033.

[24] D.E. Sosnovik, R. Weissleder, Emerging concepts in molecular MRI, Curr. Opin. Biotechnol. (2007). doi:10.1016/j.copbio.2006.11.001.

[25] B. Nabi, S. Rehman, S. Khan, S. Baboota, J. Ali, Ligand conjugation: An emerging platform for enhanced brain drug delivery, Brain Res. Bull. 142 (2018) 384–393. doi:10.1016/j.brainresbull.2018.08.003.

[26] M. Srinivasarao, P.S. Low, Ligand-targeted drug delivery, Chem. Rev. 117 (2017) 12133–12164. doi:10.1021/acs.chemrev.7b00013.

[27] R. Haag, F. Kratz, Polymer therapeutics: Concepts and applications, Angew. Chemie - Int. Ed. 45 (2006) 1198–1215. doi:10.1002/anie.200502113.

[28] R. Morphy, Z. Rankovic, Designed multiple ligands. an emerging drug discovery paradigm, J. Med. Chem. 48 (2005) 6523–6543. doi:10.1021/jm058225d.

[29] D.K. Tosh, L.S. Yoo, M. Chinn, K. Hong, S.M. Kilbey, M.O. Barrett, I.P. Fricks, T.K. Harden, Z.G. Gao, K.A. Jacobson, Polyamidoamine (PAMAM) dendrimer conjugates of “clickable” agonists of the A_3 adenosine receptor and coactivation of the P2Y14 receptor by a tethered nucleotide, Bioconjug. Chem. 21 (2010) 372–384. doi:10.1021/bc900473v.

[30] F. Ciruela, V. Fernández-Dueñas, K.A. Jacobson, Lighting up G protein-coupled purinergic receptors with engineered fluorescent ligands, Neuropharmacology. 98 (2015) 58–67. doi:10.1016/j.neuropharm.2015.04.001.

[31] M. Markovic, S. Ben-Shabat, S. Keinan, A. Aponick, E.M. Zimmermann, A. Dahan, Prospects and challenges of phospholipid-based prodrugs, Pharmaceutics. 10 (2018) 1–17. doi:10.3390/pharmaceutics10040210.

[32] K.A. Jacobson, P.R. Gpcrs, K.A. Jacobson, Functionalized congener approach to the design of ligands for G Protein-coupled receptors (GPCRs), Bioconjug. Chem. 20 (2009) 1816–1835. doi:10.1021/bc9000596.

[33] S. Federico, E. Margiotta, S. Paoletta, S. Kachler, K.-N. Klotz, K.A. Jacobson, G. Pastorin, S. Moro, G. Spalluto, Pyrazolo[4,3-*e*][1,2,4]triazolo[1,5-*c*]pyrimidines to develop functionalized ligands to target adenosine receptors: fluorescent ligands as an example, Medchemcomm. 10 (2019) 1094–1108. doi:10.1039/C9MD00014C.

[34] P. Fishman, S. Bar-Yehuda, E. Ardon, L. Rath-Wolfson, F. Barrer, A. Ochaion, L. Madi, Targeting the A_3 adenosine receptor for cancer therapy: Inhibition of prostate carcinoma cell growth by A3AR agonist, Anticancer Res. 23 (2003) 2077–2083.

[35] G. Ohana, S. Bar-Yehuda, A. Arich, L. Madi, Z. Dreznick, L. Rath-Wolfson, D. Silberman, G. Slosman, P. Fishman, Inhibition of primary colon carcinoma growth and liver metastasis by the A_3 adenosine receptor agonist CF101, Br. J. Cancer. 89 (2003) 1552–1558. doi:10.1038/sj.bjc.6601315.

[36] L. Madi, S. Bar-Yehuda, F. Barer, E. Ardon, A. Ochaion, P. Fishman, A_3 adenosine receptor activation in melanoma cells, J. Biol. Chem. 278 (2003) 42121–42130. doi:10.1074/jbc.M301243200.

[37] L. Madi, A. Ochaion, L. Rath-Wolfson, S. Bar-Yehuda, A. Erlanger, G. Ohana, A. Harish, O. Merimski, F. Barer, P. Fishman, The A_3 adenosine receptor is highly expressed in tumor versus normal cells: potential target for tumor growth inhibition., Clin. Cancer Res. 10 (2004) 4472–4479. doi:10.1158/1078-0432.CCR-03-0651.

[38] S. Gessi, E. Cattabriga, A. Avitabile, R. Gafa, G. Lanza, L. Cavazzini, N. Bianchi, R. Gambari, C. Feo, A. Liboni, S. Gullini, E. Leung, S. Mac-Lennan, P.A. Borea, Elevated expression of A_3 adenosine receptors in human colorectal cancer is reflected in peripheral blood cells, Clin Cancer Res. 10 (2004) 5895–5901. doi:10.1158/1078-0432.CCR-1134-03\r10/17/5895 [pii].

[39] E. Margiotta, S. Moro, A comparison in the use of the crystallographic structure of the human A_1 or the A_{2A} adenosine receptors as a template for the construction of a homology model of the A_3 subtype, Appl. Sci. 9 (2019) 821. doi:10.3390/app9050821.

[40] E. Kozma, T.S.S. Kumar, S. Federico, K. Phan, R. Balasubramanian, Z.-G. Gao, S. Paoletta, S. Moro, G. Spalluto, K.A. Jacobson, Novel fluorescent antagonist as a molecular probe in A_3 adenosine receptor binding assays using flow cytometry, Biochem. Pharmacol. 83 (2012) 1552–1561. doi:10.1016/j.bcp.2012.02.019.

[41] K.A. Jacobson, K.S. Thatikonda, E.E. Kozma, G. Spalluto, S. Moro, S. Federico, Fluorescent antagonists of the A_3 adenosine receptor, 9,227,979 B2, 2016. http://patft.uspto.gov/netacgi/nph-Parser?Sect1=PTO2&Sect2=HITOFF&p=1&u=%2Fnetahtml%2FPTO%2Fsearch-adv.htm&r=1&f=G&l=50&d=PTXT&S1=9,227,979&OS=+9,227,979&RS=9,227,979 (accessed March 28, 2019).

[42] S. Moro, P. Braiuca, F. Deflorian, C. Ferrari, G. Pastorin, B. Cacciari, P.G. Baraldi, K. Varani, P.A. Borea, G. Spalluto, Combined target-based and ligand-based drug design approach as a tool to define a novel 3D-pharmacophore model of human A_3 adenosine receptor antagonists: pyrazolo[4,3-*e*]1,2,4-triazolo[1,5-*c*]pyrimidine derivatives as a key study, J. Med. Chem. 48 (2005) 152–162. doi:10.1021/jm049662f.

[43] Z.G. Gao, J.B. Blaustein, A.S. Gross, N. Melman, K.A. Jacobson, N6-Substituted adenosine derivatives: Selectivity, efficacy, and species differences at A_3 adenosine receptors, Biochem. Pharmacol. 65 (2003) 1675–1684. doi:10.1016/S0006-2952(03)00153-9.

[44] E. Margiotta, G. Deganutti, S. Moro, Could the presence of sodium ion influence the accuracy and precision of the ligand-posing in the human A_{2A} adenosine receptor orthosteric binding site using a molecular docking approach? Insights from Dockbench, J. Comput. Aided. Mol. Des. 32 (2018) 1337–1346. doi:10.1007/s10822-018-0174-2.

[45] Chemical Computing Group (CCG) Inc., Molecular Operating Environment (MOE), (2016).

[46] A.D. MacKerell, N. Banavali, N. Foloppe, Development and current status of the CHARMM force field for nucleic acids, Biopolymers. 56 (2000) 257–265. doi:10.1002/1097-0282(2000)56:4<257::AID-BIP10029>3.0.CO;2-W.

[47] The Cambridge Crystallographic Data Centre (CCDC), Genetic Optimization for Ligand Docking (GOLD). https://www.ccdc.cam.ac.uk/solutions/csd-discovery/components/gold/.

[48] J. Wang, R.M. Wolf, J.W. Caldwell, P.A. Kollman, D.A. Case, Development and testing of a general amber force field, J. Comput. Chem. 25 (2004) 1157–1174. doi:10.1002/jcc.20035.

[49] H.M. Berman, J. Westbrook, Z. Feng, G. Gilliland, T.N. Bhat, H. Weissig, I.N. Shindyalov, P.E. Bourne, The Protein Data Bank, Nucleic Acids Res. 28 (2000) 235–242. doi:10.1093/nar/28.1.235.

[50] A.S. Doré, N. Robertson, J.C. Errey, I. Ng, K. Hollenstein, B. Tehan, E. Hurrell, K. Bennett, M. Congreve, F. Magnani, C.G. Tate, M. Weir, F.H. Marshall, Structure of the adenosine A_{2A} receptor in complex with ZM241385 and the xanthines XAC and caffeine, Structure. 19 (2011) 1283–1293. doi:10.1016/j.str.2011.06.014.

[51] A. Glukhova, D.M. Thal, A.T. Nguyen, E.A. Vecchio, M. Jörg, P.J. Scammells, L.T. May, P.M. Sexton, A. Christopoulos, Structure of the adenosine A_1 receptor reveals the basis for subtype selectivity, Cell. 168 (2017) 867-877.e13. doi:10.1016/j.cell.2017.01.042.

[52] J.A. Ballesteros, H. Weinstein, Integrated methods for the construction of three-dimensional models and computational probing of structure-function relations in G protein-coupled receptors, Methods Neurosci. 25 (1995) 366–428. doi:10.1016/S1043-9471(05)80049-7.

[53] Gnuplot, (n.d.). http://www.gnuplot.info/download.html.

[54] E.F. Pettersen, T.D. Goddard, C.C. Huang, G.S. Couch, D.M. Greenblatt, E.C. Meng, T.E. Ferrin, UCSF Chimera - A visualization system for exploratory research and analysis, J. Comput. Chem. 25 (2004) 1605–1612. doi:10.1002/jcc.20084.

[55] W. Humphrey, A. Dalke, K. Schulten, VMD: visual molecular dynamics., J Mol Graph. 14 (1996) 27, 33–38. doi:10.1016/0263-7855(96)00018-5.

[56] RDKit: Cheminformatics and Machine Learning Software, (n.d.). http://www.rdkit.org/.

[57] M. Head-Gordon, J.A. Pople, M.J. Frisch, MP2 energy evaluation by direct methods, Chem. Phys. Lett. 153 (1988) 503–506. doi:10.1016/0009-2614(88)85250-3.

[58] M.J. Frisch, G.W. Trucks, H.B. Schlegel, G.E. Scuseria, M.A. Robb, J.R. Cheeseman, G. Scalmani, V. Barone, G.A. Petersson, H. Nakatsuji, X. Li, M. Caricato, A. V. Marenich, J. Bloino, B.G. Janesko, R. Gomperts, B. Mennucci, H.P. Hratchian, J. V. Ortiz, A.F. Izmaylov, J.L. Sonnenberg, D. Williams-Young, F. Ding, F. Lipparini, F. Egidi, J. Goings, B. Peng, A. Petrone,

T. Henderson, D. Ranasinghe, V.G. Zakrzewski, J. Gao, N. Rega, G. Zheng, W. Liang, M. Hada, M. Ehara, K. Toyota, R. Fukuda, J. Hasegawa, M. Ishida, T. Nakajima, Y. Honda, O. Kitao, H. Nakai, T. Vreven, K. Throssell, J.A.J. Montgomery, J.E. Peralta, F. Ogliaro, M.J. Bearpark, J.J. Heyd, E.N. Brothers, K.N. Kudin, V.N. Staroverov, T.A. Keith, R. Kobayashi, J. Normand, K. Raghavachari, A.P. Rendell, J.C. Burant, S.S. Iyengar, J. Tomasi, M. Cossi, J.M. Millam, M. Klene, C. Adamo, R. Cammi, J.W. Ochterski, R.L. Martin, K. Morokuma, O. Farkas, J.B. Foresman, D.J. Fox, Gaussian 16, (2016).

[59] M.A. Lomize, A.L. Lomize, I.D. Pogozheva, H.I. Mosberg, OPM: orientations of proteins in membranes database., Bioinformatics. 22 (2006) 623–625. doi:10.1093/bioinformatics/btk023.

[60] W.L. Jorgensen, J. Chandrasekhar, J.D. Madura, R.W. Impey, M.L. Klein, Comparison of simple potential functions for simulating liquid water, J. Chem. Phys. 79 (1983) 926–935. doi:10.1063/1.445869.

[61] H. Grubmuller, V. Groll, Solvate | Max Planck Institute for Biophysical Chemistry, (1996). https://www.mpibpc.mpg.de/grubmueller/solvate (accessed August 7, 2019).

[62] H.J.C. Berendsen, J.P.M. Postma, W.F. van Gunsteren, A. DiNola, J.R. Haak, Molecular dynamics with coupling to an external bath, J. Chem. Phys. 81 (1984) 3684–3690. doi:10.1063/1.448118.

[63] R.J. Loncharich, B.R. Brooks, R.W. Pastor, Langevin dynamics of peptides: The frictional dependence of isomerization rates of N-acetylalanyl-N-methylamide, Biopolymers. 32 (1992) 523–535. doi:10.1002/bip.360320508.

[64] U. Essmann, L. Perera, M.L. Berkowitz, T. Darden, H. Lee, L.G. Pedersen, A smooth particle mesh Ewald method, J. Chem. Phys. 103 (1995) 8577–8593. doi:10.1063/1.470117.

[65] D. Sabbadin, A. Ciancetta, S. Moro, Bridging molecular docking to membrane molecular dynamics to investigate GPCR–ligand recognition: the human A_{2A} adenosine receptor as a key study, J. Chem. Inf. Model. 54 (2014) 169–183. doi:10.1021/ci400532b.

[66] A. Cuzzolin, M. Sturlese, G. Deganutti, V. Salmaso, D. Sabbadin, A. Ciancetta, S. Moro, Deciphering the complexity of ligand–protein recognition pathways using supervised molecular dynamics (SuMD) simulations, J. Chem. Inf. Model. 56 (2016) 687–705. doi:10.1021/acs.jcim.5b00702.

[67] J.C. Phillips, R. Braun, W. Wang, J. Gumbart, E. Tajkhorshid, E. Villa, C. Chipot, R.D. Skeel, L. Kalé, K. Schulten, Scalable molecular dynamics with NAMD, J. Comput. Chem. 26 (2005) 1781–1802. doi:10.1002/jcc.20289.

Highlights

- Conjugable A_3 AR ligands were synthesized to develop multi-purpose ligands
- Both amines and alkynes were used as conjugable moieties
- Conjugable ligands were used to develop AR fluorescent antagonists
- Conjugation decreased selectivity for A_3 AR leading to dual A_{2A}/A_3 AR ligands

Declaration of interests

☒ The authors declare that they have no known competing financial interests or personal relationships that could have appeared to influence the work reported in this paper.

☐The authors declare the following financial interests/personal relationships which may be considered as potential competing interests: